The Pennsylvania State University

Graduate School

College of Earth and Mineral Sciences

Use of Photolithography and Chemical Etching in the Preparation of Miniature
Piezoelectric Devices from Lead Zirconate Titanate (PZT) Ceramics

A Thesis in

Ceramic Science

by

Susan Elizabeth Trolier

Submitted in Partial Fulfillment
of the Requirements
for the Degree of

Master of Science

May 1987

Susan Elizabeth Trolier

We approve the thesis of Susan Elizabeth Trolier.

Date of Signature:

2/26/87

Robert E. Newnham, Professor of Solid State
Science, Thesis Advisor

2/20/87

L. Eric Cross, Evan Pugh Professor of Electrical
Engineering

2/20/87

Karl E. Spear II, Professor of Ceramic Science,
In Charge of Graduate Programs in Ceramic
Science

2/20/87

Carlo G. Pantano, Associate Professor of
Materials Science and Engineering

ABSTRACT

Photolithography and chemical etching were investigated as a potential means of fabricating miniature piezoelectric devices. Among the acids studied, concentrated HCl demonstrated the fastest etching of PZT-501A disks over a wide temperature range. This rate is believed to be due to the fact that the acid is a grain-boundary specific etchant so that it dissolves the material around the grains, freeing rather than etching through them. HCl also proved to be compatible with some commercially available photoresists and so could be incorporated into a simple experimental procedure for delineating and etching patterns in the ceramic.

Using this technique, several piezoelectric devices were manufactured from thin (~0.2mm thick) ceramic wafers. Flexural mode resonators similar to tuning forks were generated with fundamental resonances between 10 and 115 kHz. These same devices were then used to provide simultaneous measurements of the density and viscosity of liquids by monitoring the position of the resonance frequency and the width of the resonant peak, respectively. Thickness extensional resonators with reduced planar coupling were also fabricated by etching a thin spiral through the thickness of a ceramic disk. This ability to selectively destroy lateral resonances could make high frequency (>2 MHz) PZT transducers for medical imaging systems feasible. Finally, folded ultrasonic delay lines were fabricated by etching PZT disks into planar spirals. These should prove valuable as compact variable delay lines.

This processing technique is not materials specific, and so should be useful for processing complex two-dimensional configurations from a variety of substrate materials.

TABLE OF CONTENTS

LIST OF TABLES

LIST OF FIGURES

ACKNOWLEDGEMENTS

Chapter 1

INTRODUCTION

1.1 Objectives

The technology necessary for the production of miniaturized devices has been developed for and is universally exploited by the semiconductor industry in the production of integrated circuitry. Although many other fields could benefit from the ability to microfabricate components, little work has been done to transfer the available knowledge to other systems. Thus, the first objective of this study was to determine if the photolithographic process could be adapted to ceramic materials.

The second objective of this work was to use the technique to manufacture piezoelectric devices which would be difficult or impossible to replicate by available methods. Ferroelectric lead zirconate titanate (PZT) was chosen as the substrate material because miniature piezoelectric devices could be employed as resonators or sensors.

Practically, the first objective implied that a suitable chemical etchant for PZT and a compatible photoresist had to be found. Consequently, a survey of the etching rates of the ceramic in various caustic liquids was undertaken with the intent that a commercially available photoresist would be chosen to match the most promising. Once such a system had been determined, studies which would outline the range of device dimensions obtainable using the processing technique were planned.

In pursuing the second objective it was decided that as many potential devices as possible would be studied. This would demonstrate the flexibility of the technique while simultaneously testing its limitations. Among the devices chosen for investigation were flexural and thickness mode resonators and acoustic delay lines.

1.2 Fabrication Process

1.2.1 Microfabrication of Silicon

1.2.1.1 Microelectronics

The advent of the microcomputer was presaged by the development of a fabrication procedure which permitted the semiconductor industry to mass produce miniature electronic devices. This technology, and hence the whole realm of integrated circuit manufacture hinges on the ability to create very fine patterns on the surface of a silicon wafer by selectively removing minute quantities of material. In order to accomplish this, a multi-step process is employed wherein a pattern masking portions of the wafer surface is first delineated so that unprotected areas can later be etched away (1). The process, pictured in Fig. 1, is thus largely analogous to the production of pictures by the printing plate method. For many applications in microelectronics the photoresist is used only to pattern a design in a thin layer of SiO_2 grown on the surface of the chip. This film then serves as the resist for all subsequent etching steps.

Replication of a desired pattern, or lithography, by conventional methods necessitates the use of an energy sensitive barrier, called a resist, and an activating light source. Most commonly, the photoresist is applied by dropping a small amount of liquid on to the wafer surface and then spinning the disk at very high speeds (3000 - 6000 rpm is typical (2)) to spread the fluid into a thin, even coating. Once this is done, the coated disk is soft-baked to remove the solvent from the liquid film (3). Dried disks are then exposed by projecting an intense light through a photomask patterned with the circuit design. This affects the photoresist in one of two fashions, depending on the type utilized. Negative resists are polymeric compounds composed of a photosensitive material and a synthetic-rubber component. Upon exposure to light, the photoresist undergoes
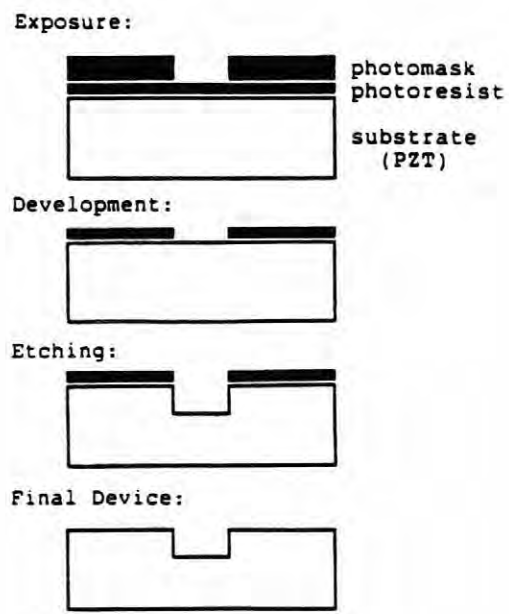
Fig. 1: Photolithography process

a chemical reaction in which the photoactive material, bis-aryldiazide, cross-links the rubber, rendering it insoluble in the developing solution. Consequently, on developing, only the unexposed regions dissolve, and the desired pattern is produced (3). Positive resists, on the other hand, contain three components, a photoactive compound, a resin, and a solvent. During exposure to radiation, the photoactive compound, O - naphtha-quinonediazide, hydrolizes and decomposes into carboxylic acid. Thus, when developed in a basic solution, the exposed areas dissolve (See Fig. 2) (3). For the unexposed regions the material acts as an inhibitor, preventing etching of the low molecular weight Novolak resin.

Projection of light through the photomask can be accomplished in two distinct fash-ions. In the first, contact printing, the mask transparency is laid directly on top of the resist-coated wafer. While this technique eliminates many potential difficulties due to slightly uneven wafer surfaces, it is used only rarely because it leads to rapid deteriora-tion of the patterned mask. (Contact with the resist results in abrasion defects which are then printed with all subsequent uses of the film.) The combination of these unavoidable defects with diffraction effects limits the resolution of contact lithography to 2-7μm, although 0.5μm linewidths have occasionally been achieved using deep UV radiation (1).

A technique which is more frequently encountered is projection printing, where a high resolution lens is used to focus incident light through the mask onto the wafer (4). As this process does not necessitate contact between the photomask and the wafer, accu-mulated defects are not problematic. Resolution is, however, limited to 3μm by scatter-ing of light through the lens, mechanical vibration, airborne contamination, imperfect wafer surfaces, and diffraction effects (4).

Because diffraction limits resolution by a factor proportional to

$$\frac{\lambda}{\text{numerical aperture}}$$

(5) to procure finer resolution it is necessary to utilize radiation with a wavelength shorter than that of visible light. For this reason, both x-ray and charged-particle
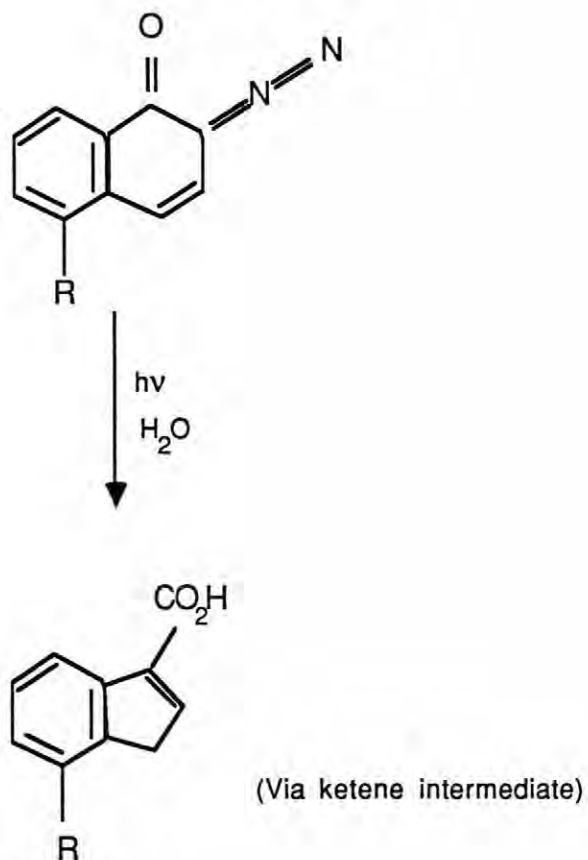
Fig. 2: Decomposition of the photoactive compound in a positive resist (3)

lithographies are essential in the production of densely packed chips. Using a poly (methylmethacrylate) resist which depolymerized on exposure to x-rays, Smith et. al. (6) reported resolution of 0.5μm. Similarly, patterns of remarkable clarity (resolution of 0.1μm) are reported using electron beams (1). Finally, ion beam lithography, the newest technique, possesses resolution comparable to the electron beam method, and so it is useful both in direct wafer writing and in mask fabrication.

It should be noted that the extremely fine feature sizes cited here can be achieved only under strict clean room conditions (7-9). Dust particles which adhere to the wafer surface, for example, can seriously mar the photolithographic pattern. Consequently, particles of only 10-30% of the desired linewidth can result in imperfections with effects as varied as "marginal changes in circuit parameters and a tendency towards degraded performance to outright catastrophic failure of the finished component" (7).

Once the pattern has been delineated in the resist, the design must somehow be engraved into the substrate. Most frequently, this is accomplished using wet chemical etching, but ion etching and reactive plasma etching are now utilized when either high resolution or special microstructural features are demanded.

In order to implement chemical etching, it is necessary to find a reagent which readily dissolves the substrate while leaving the patterned resist intact. Two distinct types of etchants are utilized in the microfabrication of silicon wafers: isotropic etchants which attack all crystallographic directions at the same rate and anisotropic etchants for which the etching rate is a function of the Miller indices of the plane.

Due to their selectivity, anisotropic etchants are used to formulate the most precise and demanding geometries. Because the morphology of the etch trenches is determined by the slowest etching face, sidewalls of features meet at well defined and highly reproducible angles (corresponding to the family of {111} planes for (100) silicon). Using a solution of 4 mole % pyrocatechol, 46.4 mole % ethylene diamine, and 49.4 mole % water as an anisotropic etchant for silicon in the production of integrated circuitry, Bean (10)

effected packing densities of <1μm and etching ratios of 650 to 1.

Although chemical etching is widely applied in the semiconductor industry, its use is bounded by a tendency to bridge between closely spaced strips of photoresist, prohibiting etching in that channel. Thus, to obtain very fine microstructures, either ion or reactive plasma etching must be employed. The first of these, ion or sputter etching, entails the use of energetic argon ions as a bombarding species active enough to dislodge Si atoms from their lattice sites. Since most materials possess similar sputter yields, however, ion milling will not be useful until a means is devised to deflect the beam precisely, forestalling the need for masks (1). Of more immediate practical concern then, is reactive plasma etching. In this technique, the wafer is placed in a reactive gas ambient, but no high voltage acceleration of the ions is attempted. Instead, the substrate is removed as a gaseous species absorbs, undergoes a chemical reaction, and desorbs as a silicon containing gas.

i.e.

$$CF_4 \longrightarrow CF_2 + 2F$$
$$Si_{(s)} + 4F \longrightarrow SiF_{4(g)}$$
$$SiO_{2(s)} + 4F \longrightarrow SiF_{4(g)} + O_2$$
$$Si_3N_{4(s)} + 12F \longrightarrow 3SiF_{4(g)} + 2N_2$$
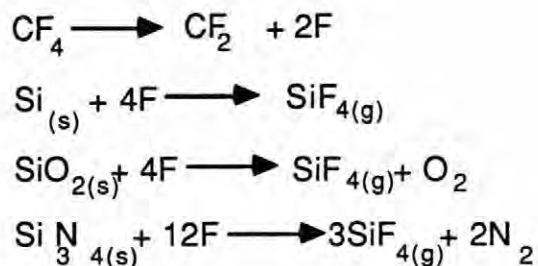
Wang and Wong (11) have attained aspect ratios (depth of trench divided by the width of the opening) ranging from 2:1 to 10:1 or greater in research on trench etching techniques for dielectric isolation using this process. Plasma etching was also utilized by Takahashi, Murai, and Kodera (12) to fabricate submicrometer gates for GaAs MESFET's.

1.2.1.2 Micromechanical Devices

The same techniques exploited in the manufacture of integrated circuitry have also been used to produce miniature mechanical devices from silicon wafers. This type of

micromachining has resulted in inkjet nozzles, multisocket electrical connectors, multi-channel arrays and wave-guides, pressure sensors, valves, and gas chromatographs (13,14) with feature sizes almost as small as those realized in microelectronics. In addition to the tremendous size advantage devices of this kind exhibit over their full-scale counterparts, the fact that their processing is compatible with the production of microcircuits makes them particularly amenable to integrated packages.

Micromachining relies almost exclusively on the use of anisotropic etchants to define the device geometry. Because the rate of attack varies widely along the different crystallographic planes of silicon (Bassous reports 50, 30, and 1 μm per hour for the {100}, {110}, and {111} planes respectively (14)) etched cavities grow until bound by a combination of {111} and {110} walls. Consequently, with careful orientation of the photolithographic pattern on the substrate wafer, it is possible to assure trenches with perpendicular or pyramidal sidewalls. Using this technique, Bassous fabricated nozzles for inkjet printers, electrical connectors, and optical waveguides (14). Similar work at the Integrated Circuits Laboratory at Stanford University and at IBM have produced numerous other devices including pressure sensors, accelerometers, and heat sinks for microchips (13). Among the most elaborate of the microprocessed devices fabricated thus far is the gas chromatograph pictured in Fig. 3.

1.2.2 Microfabrication of Ceramics

1.2.2.1 Quartz piezoelectrics

One of the few instances in which photolithography and chemical etching have been applied to non-semiconducting materials is in the production of quartz devices for frequency control. Many quartz wristwatches, for example, rely on miniature tuning forks made in this way (15,16). The technique is particularly suited to device fabrication of
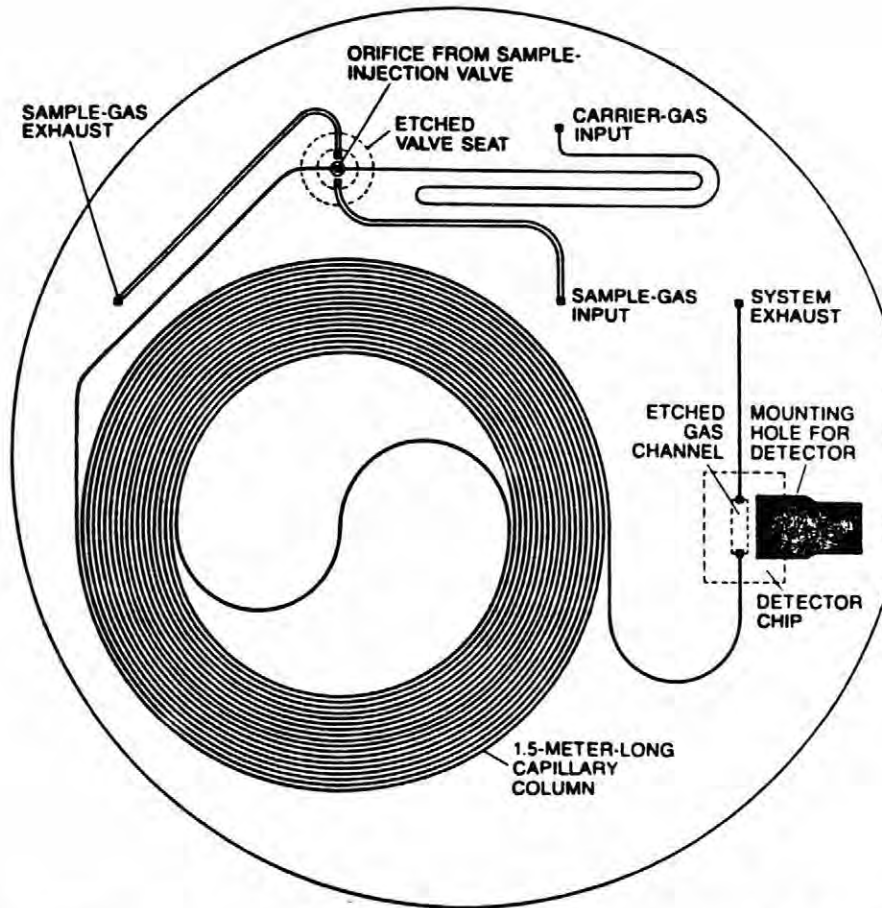
"Separation of gases in the silicon gas chromatograph is based on the differences in the solubility of various gases in a liquid that lines the capillary column. An inert carrier gas flows continuously through the capillary-column channel. When a valve in the channel is opened, a pulse of the gas to be analyzed is fed into the column and flushed through it by the carrier gas. As the gases in the sample pass through the column they are repeatedly absorbed and desorbed on a thin liquid lining. Each gas is identified by its retention time in the column. As each gas arrives in turn at the end of the column, it passes through a hole to a channel on the back of the wafer over which a thermal-conductivity detector is mounted. Sample gases have a lower thermal conductivity than the helium carrier gas has and cause voltage peaks in the detector output. The volume of each gas is determined from the area under the voltage peak it creates."

Fig. 3: Miniature gas chromatograph (13)

this type because it permits inexpensive mass-production of precision components. This same reasoning is operant in the use of photolithography and etching for the manufacture of surface acoustic wave (SAW) resonators. In this case, an array of fine grooves is etched on each side of two interdigital transducers (See Fig. 4) to reflect surface waves for a range of frequencies. Again, the substrate is SiO_2.

1.2.2.2 Perovskite Ferroelectrics

The only application of micromachining to ferroelectric ceramics found in the literature was the work by Shiosaki and his co-workers on laser enhanced chemical etching of PZT and $PbTiO_3$ (17,18). In their experiments, an Ar^+ laser focussed on the surface of a ceramic disk immersed in a 10 $^{mol}/_l$ KOH, water solution was used to etch both trenches and holes. The initial etching rate of >100 μm per second is exceedingly high, but it dropped off rapidly (Fig. 5) due to disruptions in the laser power transmission through the KOH layer and defocussing of the laser at increased etch depths. At this etchant concentration etching is reported to occur intergranularly rather than by melting and refreezing of the surface.

Aside from this work, little has been reported even on the etching rates of the ferroelectrics in various liquids. Consequently, Solubilities of Inorganic and Organic Compounds (19) lists no data on any zirconates or titanates. The richest source of information on the etching of perovskites, then, was papers by microscopists interested in delineating either grain or domain boundaries by chemical etching. A compilation of the compositions utilized is given in Table 1.

In almost all cases these constituted light etches of the ceramics with etching times of only one to ten minutes. It was expected that use of such chemical etchants for the micromachining of PZT would require longer times and harsher etching conditions.
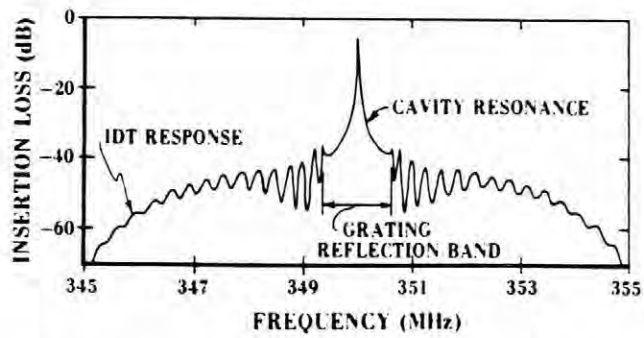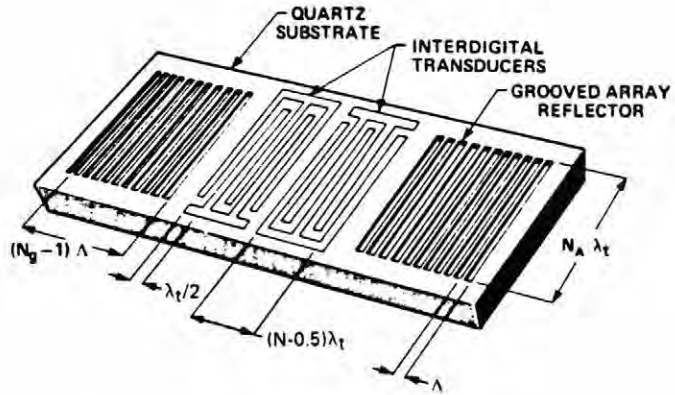
Fig. 4: SAW resonator (15)
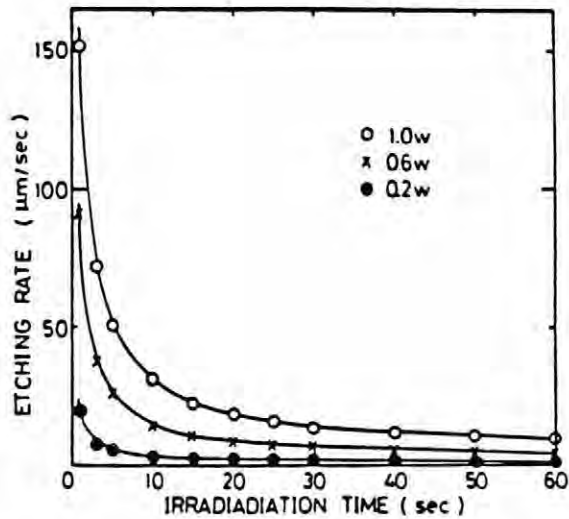
Fig. 5: Laser enhanced etching of PZT (18)

Table 1: Compositions used in the etching of perovskites

Perovskite	Etchant	Reference
$BaTiO_3$	HCl	(20)
$BaTiO_3$	1 drop HF in 5cc water	(20)
$BaTiO_3$	cold concentrated HCl	(21)
$BaTiO_3$	0.5% HF and HNO_3	(22)
$BaTiO_3$	HCl, room temperature	(23)
$BaTiO_3$	orthophosphoric acid 130-150°C	(24)
$BaTiO_3$	$BaCl_2$ and NaOH salt solutions at high temperature	(24)
$SrTiO_3$	HF:$2HNO_3$: $2H_2O$	(25)
PZT	hot concentrated H_3PO_4	(26)
PZT	0.50-$9.20^{mol}/_l$ HNO_3, 0.03-$3.00^{mol}/_l$ fluoride ion, balance H_2O	(27)
PLZT	5% HCl with 7 drops 35% HF	(28)

1.3   Microprocessed Ferroelectric Devices

1.3.1 Flexural Mode Resonator

1.3.1.1 Geometry and Electrode Pattern

A bar of any material can be made to flex if one side is forced to expand while the opposite contracts. (See Fig. 6) When this motion is made periodic, the bar vibrates at some natural frequency determined both by its dimensions and by the speed with which an acoustic wave travels through the medium. For a long, thin bar clamped on one end, this frequency is given by the Euler beam formula:

$$f_r = \frac{\beta^2}{2\pi\sqrt{12}} \frac{w}{l^2} \sqrt{\frac{E}{\rho}}$$

(29,30) where f_r is the resonant frequency, w is the cantilever width, l the cantilever length , E the elastic modulus, ρ the density and β^2 depends on the order of the resonance and the ratio w/l. Thus, for a thin beam, $\beta_1 = 1.875$, $\beta_2 = 4.694$, and $\beta_3 = 7.855$.

Similar resonators can be made out of piezoelectric ceramics if some electrode pattern which induces flexure in the bars is used. Both quartz (16) and $PbTiO_3$ (29) tuning forks have been made using the configurations shown in Fig. 7.

In this study, a slightly different geometry for the resonating element was chosen. Four cantilevers arranged around a center bar so that the whole looked like a capital "H" (See Fig. 8) would be etched out of a sheet of PZT poled in the thickness direction. With one face electroded as demonstrated in Fig. 9 and the other completely metallized and allowed to act as a floating electrode, an electric field like that of Fig. 10 would be established. Due to the converse piezoelectric effect $\varepsilon_i = d_{ij}E_j$ (31), a strain field arises in which one half of the leg expands and the other contracts. This fulfills the condition for flexure, and the cantilevers wag in the horizontal plane. By utilizing four cantilevers
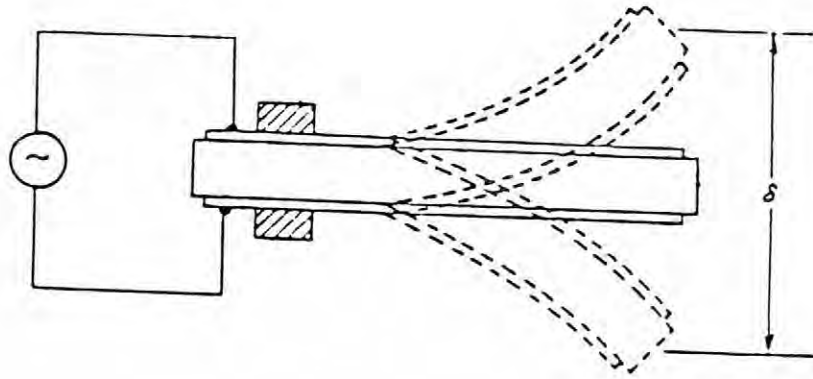
Fig. 6: Flexure of a bar (32)
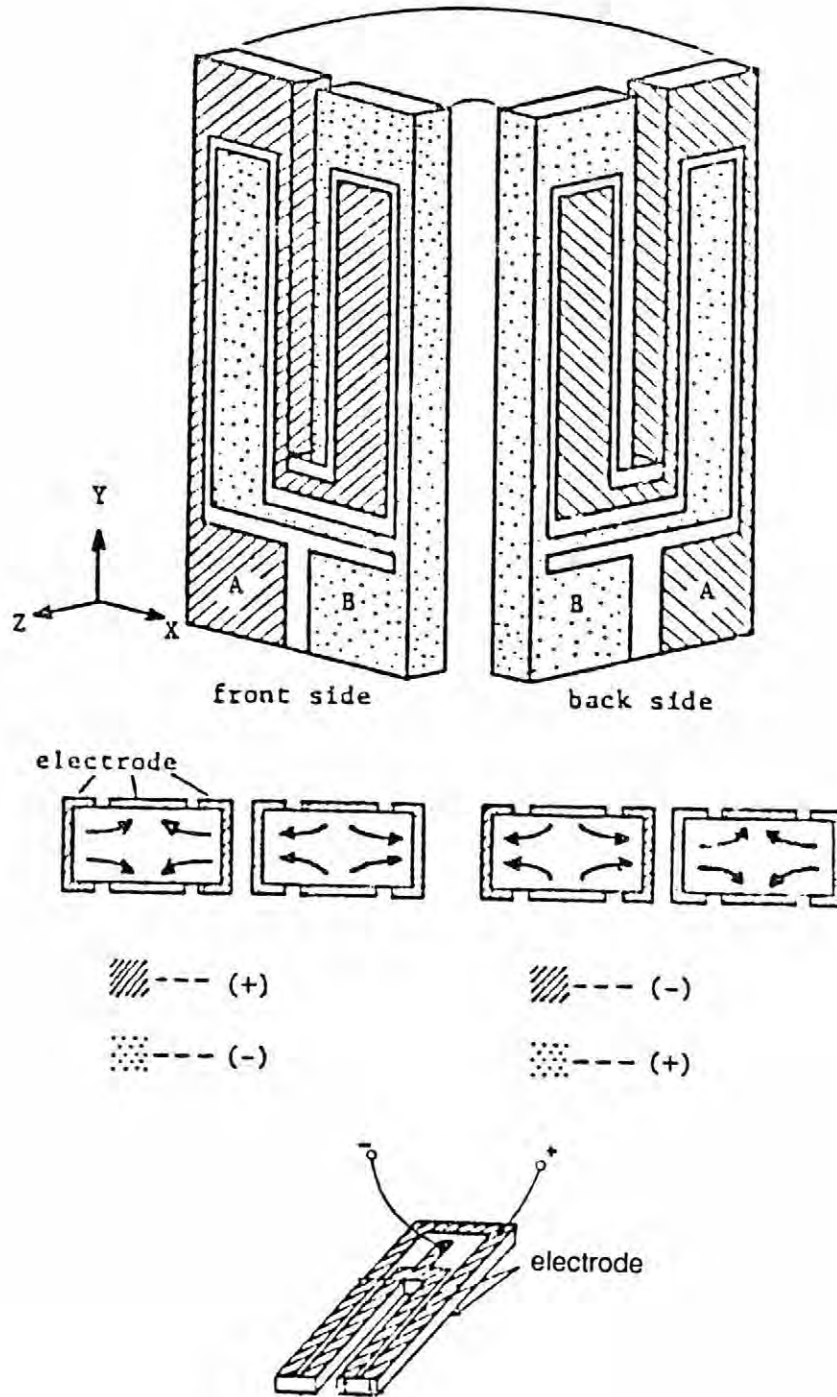
Fig. 7: Electrode patterns of commercial piezoelectric resonators (16),(29)
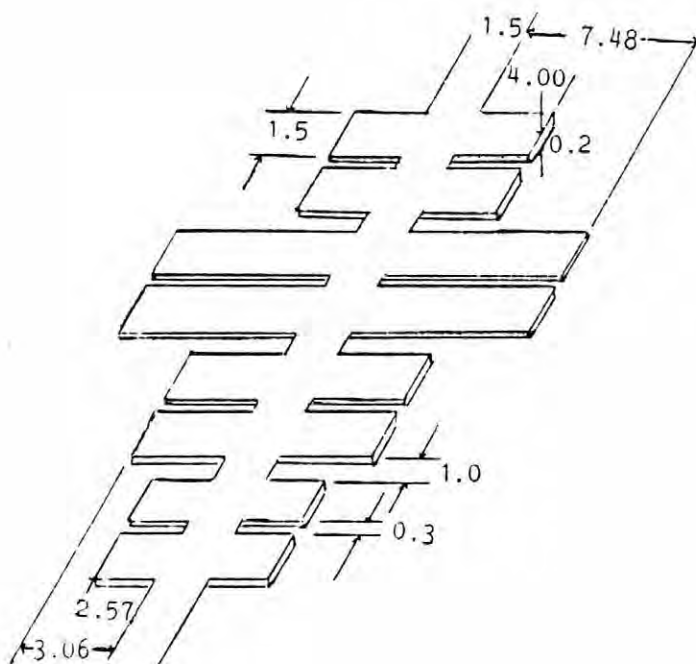
Fig. 8: Schematic of four flexural resonators (dimensions in mm)
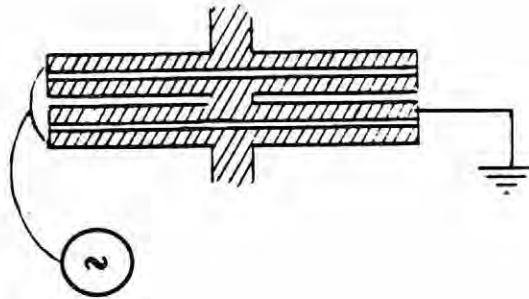
Fig. 9: Electrode pattern for flexural mode resonator
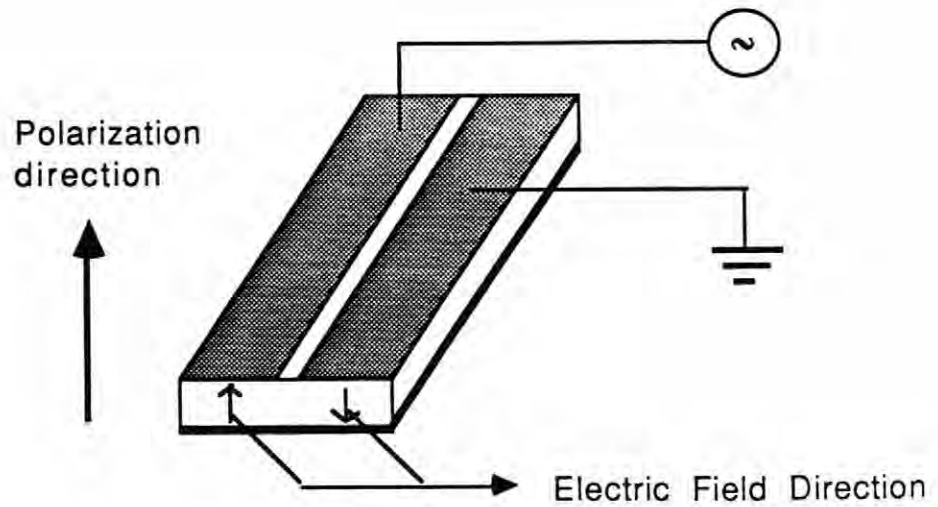
Fig. 10: Electric field established by electrode pattern

arranged so that they are symmetric about the center bar, the root of each cantilever is effectively clamped by the motion of the others. This then permits each of the cantilevers to act as though fixed on one end.

1.3.1.2 Tuning fork

Use of a device like that described in section 1.3.1.1 as a tuning fork is fairly straightforward. When the electric field is applied at the resonance frequency of the cantilevers, the device vibrates with maximum amplitude. The characteristics of the resulting resonance can be determined by monitoring its electrical properties: capacitance, impedance, conductance, etc., as the exciting field is passed through resonance (33).

The shape of the resonance is most frequently described by Q_m, the mechanical quality factor, where

$$Q_m = \frac{f_r}{\text{width of peak at half height}}$$

(34). Materials with a high mechanical quality factor, e.g. quartz, possess resonance peaks which are very narrow; lower Q materials demonstrate much broader peaks. (See Fig. 10) Since PZT 501A has a $Q_m = 80$, (35) it is expected that the resonance curve should be moderately sharp.

Tuning forks are generally designed to vibrate with a very specific, reproducible frequency. One instance where this is mandated, for example, is when the period of oscillation is used as a measure of time. Quartz oscillators are now used as in this way as secondary timing standards. Recently, similar resonators have been incorporated into wristwatches.
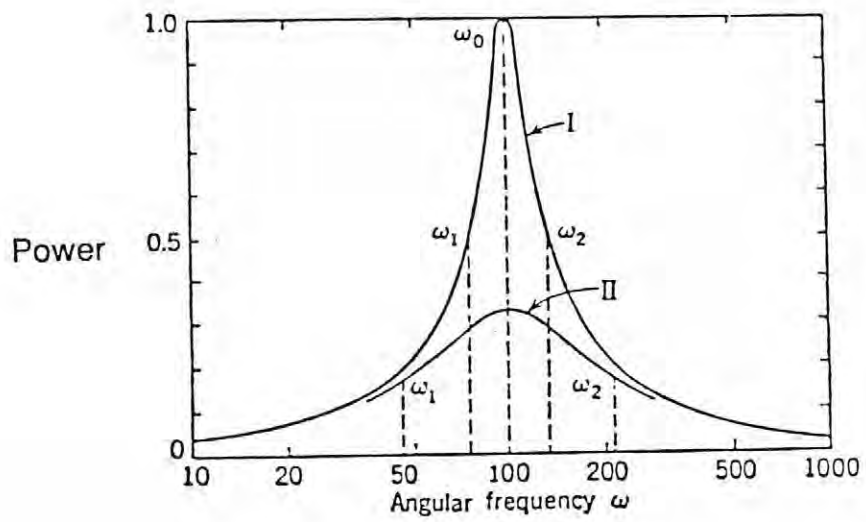
Fig. 11: Resonance curves for a simple mechanical system. (Curves I and II correspond

to $Q_m = 3$ and 1 respectively.) (34)

1.3.1.3 <u>Density Meter</u>

Whenever a transducer is excited in a fluid medium, an effective mass is forced into oscillatory motion. This quantity includes contributions from the transducer itself, i.e. the piezoelectric and the electrode, and an additional term known as the radiation mass due to the displaced fluid surrounding the ceramic. For vibrations in air, this radiation mass is very small, and so in many circumstances is considered negligible. In the case of a transducer vibrating in a liquid, however, the weight of the disturbed fluid cannot be neglected and so the effective mass is far higher.

As an approximate treatment of the effect of the mass-spring damping on the system, consider the resonance of the transducer in air to be undamped (a valid assumption for a high Q_m transducer) so that it follows the equation

$$m\frac{d^2x}{dt^2} + sx = 0$$

(34),(36) where m is mass, x is position, t is time, and s the spring stiffness constant. Solution of this equation gives the resonant frequency in terms of s and m:

$$f_r = \frac{1}{2\pi}\sqrt{\frac{s}{m}}$$

(34). For vibrations in air, m includes only the mass of the transducer and the resonance can be expressed as

$$f_r = \frac{1}{2\pi}\sqrt{\frac{s}{B\rho_{ceramic}}}$$

for B = constant and $\rho_{ceramic}$ = density of the ceramic. When the oscillator is immersed in a liquid, however, the mass of the transducer is augmented by that of the displaced fluid, m_l, so that

$$f_r = \frac{1}{2\pi}\sqrt{\frac{s}{m + m_l}}$$

Since $m_l = A \times \rho_{liq}$ and $m = B \times \rho_{ceramic}$ for A and B constant, the equation can be expressed as

$$f_r = \frac{1}{2\pi}\sqrt{\frac{s}{A\rho_{liq} + B\rho_{ceramic}}}$$

$$\frac{1}{f_r^2} = C\left[A'\rho_{liq} + B'\rho_{ceramic}\right]$$

when λ, the wavelength of the vibration in the fluid, is much greater than the size of the transducer (A', B' and C are constants). (If this last condition is not fulfilled, the trans-ducer is no longer considered a point source of radiation, and m_l becomes frequency dependent.) For cases in which the equation does hold, however, it is clear that a plot of f_r^{-2} versus ρ_{liq} should yield a straight line.

From this treatment it would be expected that a flexural mode resonator would undergo shifts in the resonant frequency when oscillated in liquids of different densities. By calibrating this change, the device could be useful as a density meter.

1.3.1.4 Viscometer

In addition to the effect of fluid on the value of the resonant frequency, the nature of the surroundings also influences the shape of the resonance peak, and hence Q_m. This in-teraction is due to the fact that during transmission of acoustic waves, some media absorb the energy more rapidly, dissipating it as heat. To derive the effect of the viscosity of the liquid on Q_m, consider the wave equation

$$\rho\frac{\delta^2 u}{\delta t^2} = q\frac{\delta^2 u}{\delta x^2} + \eta\frac{\delta^3 u}{\delta x^2 \delta t}$$

(37) where ρ = density, u = displacement, t = time, q = real elastic constant, and η = coefficient of viscosity defined as

$$\eta = v' + \frac{4}{3}v''$$

where v' = volume coefficient of viscosity and v'' = shear viscosity. This can be rewritten as

$$\rho\frac{\delta^2 u}{\delta t^2} = q\frac{\delta^2 u}{\delta x^2} + \eta\frac{\delta^2}{\delta x^2}(\frac{\delta u}{\delta t})$$

For harmonic oscillations:

$$u = u_o e^{j\omega t}$$

$$\frac{\delta u}{\delta t} = j\omega u_o e^{j\omega t}$$

$$\frac{\delta u}{\delta t} = j\omega u$$

Substitution into the wave equation gives

$$\rho\frac{\delta^2 u}{\delta t^2} = q\frac{\delta^2 u}{\delta x^2} + \eta\frac{\delta^2}{\delta x^2}(ju\omega)$$

$$= q\frac{\delta^2 u}{\delta x^2} + \eta j\omega\frac{\delta^2 u}{\delta x^2}$$

$$= \frac{\delta^2 u}{\delta x^2}(q + j\omega\eta)$$

$$= \frac{\delta^2 u}{\delta x^2}q\left[1 + \frac{j\eta\omega}{q}\right]$$

Rewriting the elastic constant as a complex quantity gives

$$q^* = q + jq' = q(1 + j\frac{q'}{q})$$

Since this is alternatively defined as

$$q^* = q(1 + j\tan\delta) = q(1 + j\frac{1}{Q_m})$$

(38) it is clear that

$$\frac{\eta\omega}{q} = \frac{1}{Q_m}$$

This final equation suggests that a piezoelectric resonator should make an accurate viscometer. Thus, with correct calibration, analysis of the resonance behavior (peak position and peak width) of an oscillator vibrating in a fluid should simultaneously provide measurements of the liquid density (section 1.3.1.3) and viscosity.

1.3.2 Thickness Mode Resonators

1.3.2.1 <u>Disk Transducers</u>

Thin, circular disks of piezoelectric ceramics are used in many applications to generate acoustic waves (39-42). For a plate poled in the thickness [3] direction and electroded on the faces, several resonance modes can be stimulated by applying an alternating voltage. The most commonly employed mode of resonance is the thickness extensional vibration in which the disk undergoes a strain corresponding to

$$\epsilon_3 = d_{33}E_3$$

(31) where ϵ_3 and E_3 correspond to the strain and electric field components in the thickness direction and d_{33} is the converse piezoelectric coefficient. For this type of motion in an infinite plate the resonance frequencies are given approximately by

$$f_n = \frac{nv}{2t}$$

for $f_n = n^{th}$ order resonance frequency, n = integer, v = velocity of an acoustic wave, and t = thickness (43). It has been shown that in the case of a piezoelectric disk, the higher harmonics are not integral multiples of the fundamental (44-45).

Because many poled ceramics such as PZT exhibit an appreciable d_{31} component of the converse piezoelectric coefficient matrix, application of an electric field along the [3] axis results in a strain along the plane of the disk also given by

$$\epsilon_1 = d_{31}E_3$$

These coupled strains cause lateral, or in the case of a circular disk, radial mode vibrations. The resonance frequencies at which these breathing modes appear are given by

$$\frac{\dfrac{\omega a}{v} J_0\left[\dfrac{\omega a}{v}\right]}{J_1\left[\dfrac{\omega a}{v}\right]} = 1 - \sigma^p$$

where ω = angular resonant frequency, a = radius of disk, v = acoustic velocity, σ^p = planar Poisson's ratio, and J_0 and J_1 are Bessel functions of the first kind of the zero and first orders respectively (46). Full equations for the resulting displacements are given by Gazis and Mindlin (47).

In many cases these radial modes are considered undesirable because they introduce additional resonances near the desired thickness resonance (48-50). Such spurious vibration modes lead to inferior device performance for several reasons. In medical imaging systems transducers with high planar coupling coefficients demonstrate extended ring down times so that single pulses become undesirably long. This in turn lowers the range resolution of a pulse-echo imaging system (48), (50,51). Similarly, lateral vibrations are detrimental to the operation of acoustic microscopes as they lead to acoustic noise (52).

Several schemes to sidestep this problem have been investigated, including manufacture of 1-3 PZT/polymer composites (33), (53,54) and the introduction of low planar coupling ceramics like $PbTiO_3$ (39), (48-50), (52). In the case of the 1-3 composite, the PZT is diced into small pillars and backfilled with a polymer. As the polymer interrupts the integrity of the PZT, it reduces the lateral coupling. This works well so long as $^w/_t$, the ratio of the width of the PZT pillar to its thickness, is less than unity. Problems do arise, however, when transducers of this type are operated at higher frequencies (i.e. >5MHz) because the microstructure is then no longer sufficiently fine ($^w/_t$ >1) to prevent lateral running modes from interfering with the thickness reso-

nance (53), (55, 56). Due to limitations in cutting and dicing, this 5MHz limit for operation appears fixed.

The second approach to eliminating lateral resonances has been the introduction of materials with low planar coupling coefficients, such as the modified lead titanates and lead zirconates. Compositions in which the thickness coupling coefficient is an order of magnitude larger than the planar coupling have been achieved in both systems (39), (48-50), (52) leading to replacement of PZT ceramics with these newer materials. Although these materials do diminish the restrictions on the high frequency operation of medical imaging systems ($^w/_t$ can be >1), implementation of such transducers is accompanied by some difficulties. The most important of these are that the modified ceramics demonstrate smaller dielectric constants, thickness coupling coefficients, and piezo-electric constants than members of the PZT family (48,49), (52,53). Consequently, they are neither as efficient in the conversion of electrical to mechanical energy nor as compatible with the driving and receiving electronics (53).

1.3.2.2 Modified Disk Transducers

In an attempt to produce a resonator from PZT with reduced radial coupling, a modified disk transducer was designed. The intent of the alteration was to destroy the symmetry of the circular wafer and so prevent the appearance of selected vibration modes. Photolithography and chemical etching are particularly suited to this task because irregular geometries are easy to obtain by this method. Cutting of the desired shape, on the other hand, is appropriate primarily for rectilinear configurations and so reduces the latitude of potential designs.

The pattern chosen to test this hypothesis was a disk transducer etched completely through the thickness with a thin spiral extending from the center to 0.77a (See Fig. 12). As in the case of an unmodified disk it would be poled in the thickness direction and
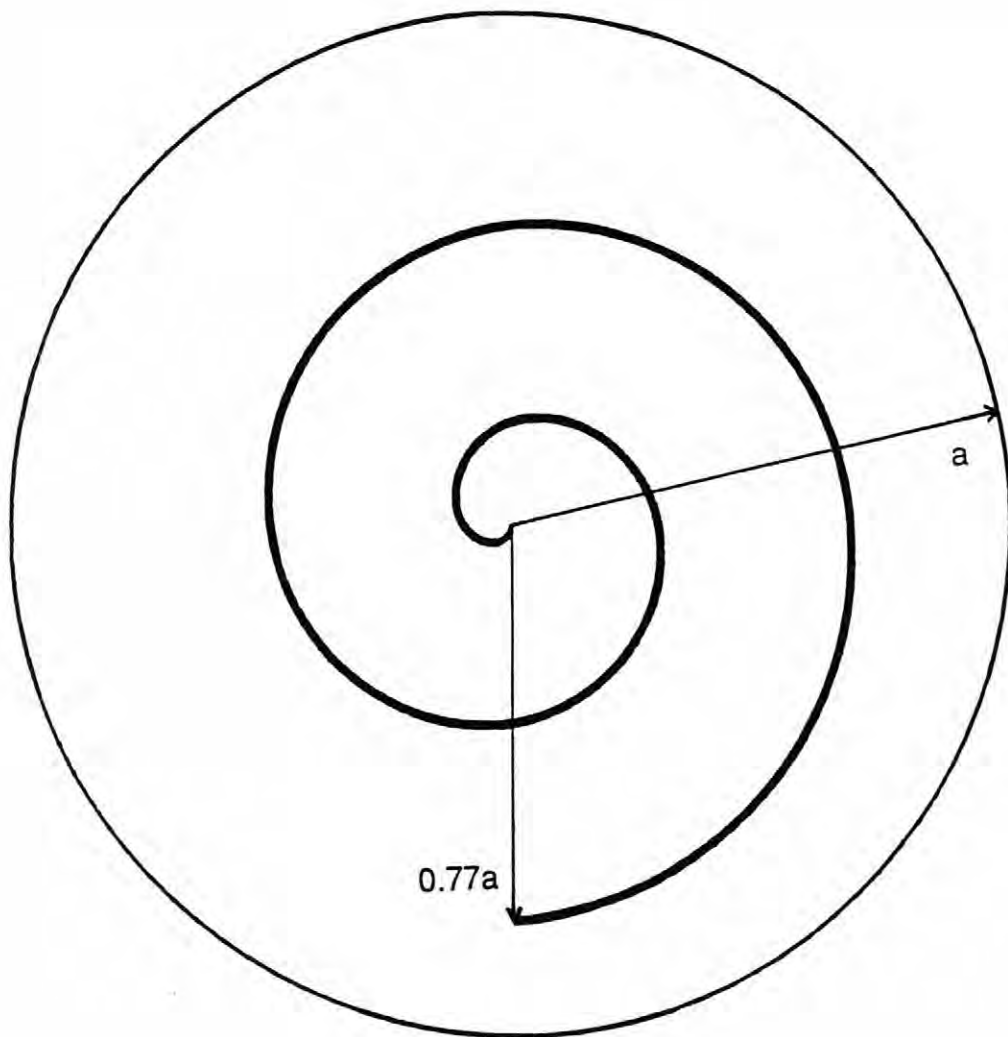
Fig. 12: Design of modified disk transducer

completely electroded on both faces. It was hoped that this would result in the elimination of the first radial mode of the disk.

1.3.3 Delay Line Devices

Delay line devices involve a very straightforward application of piezoelectricity. The idea centers on pulsing an electric signal into a piezoelectric transducer coupled to some solid medium. As the ceramic is ferroelectric, the electrical pulse is converted to an acoustic wave which propagates down the bar until at the other end a second transducer reconverts the signal to electrical energy. Because it takes a finite time for the sound wave to reach the far end of the ceramic, the electrical signal is delayed (57, 58).

The speed with which the acoustic wave moves through any medium is determined by the elastic constants. For a solid bar, the rate is given by

$$v = \sqrt{\frac{E}{\rho}}$$

(43) where v = acoustic velocity, E = Young's modulus, and ρ = density.

If one were to consider manufacturing a delay line solely from the ferroelectric PZT, the acoustic velocity would be $v = 2881 \, ^m/_s$ (59). Unfortunately, in the case of PZT, delays of $64 \mu s$, a figure common in television circuits (58), would then require a length of 18.4 cm. As it would clearly be impractical to incorporate such an unwieldy (and fragile) component into most sets, adoption of a straight piezoelectric delay line can be discounted. Through the use of a microfabrication process, however, the possibility of etching a folded delay line from a thin sheet of ceramic becomes feasible. The design chosen to test the possibility of a compact piezoelectric delay line is pictured in Fig. 13. In this configuration, a thin PZT disk poled in the thickness [3] direction is patterned with a spiral and etched. With both faces of one end electroded, a voltage can be pulsed into the bar. Due to the non-zero d_{33} component of the ceramic, this results in a strain parallel to the applied voltage corresponding to $\varepsilon_3 = d_{33}E_3$ (31). Since PZT also demonstrates
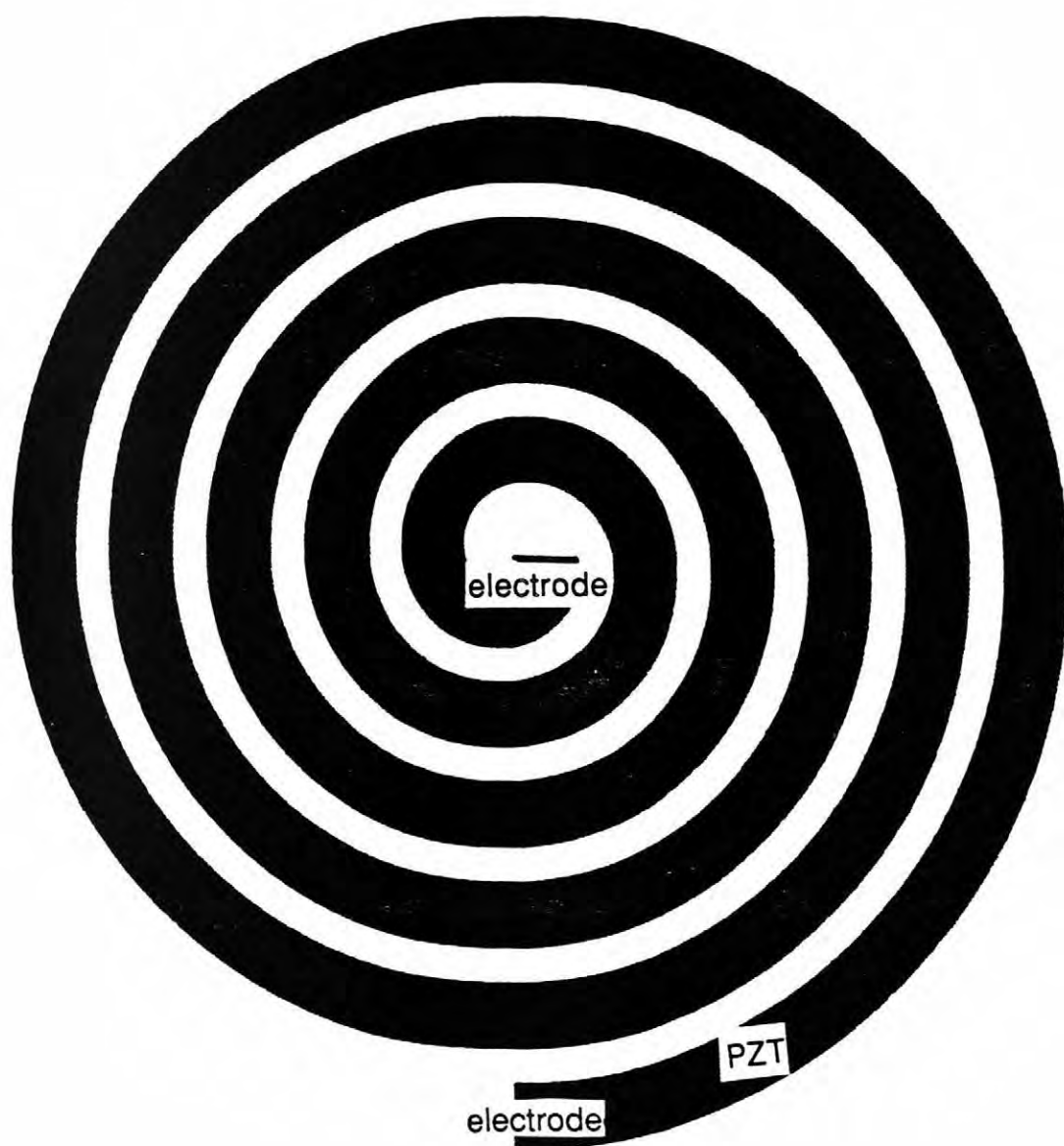
Fig. 13: Piezoelectric delay line

an appreciable d_{31}, a strain wave also propagates down the length of the bar, perpendicular to the applied field via $\epsilon_1 = d_{31}E_3$. It is this wave which underlies the delay line behavior as after circling the length of the spiral, the d_{31} induced strain can be reconverted to an electrical pulse by a matching set of electrodes on the far end.

This configuration is especially useful for several reasons. Like SAW devices, it is fabricated from a single material and hence there is no discontinuity between the exciting and receiving transducers and the medium carrying the acoustic wave. Consequently, the device can be made into a variable delay line by placing several taps along the propagation length. Secondly, PZT has a high electromechanical coupling coefficient and so should demonstrate a large bandwidth, a feature which is difficult to attain in SAW devices (58).

The one serious drawback to a continuous PZT delay line is that the ceramic is not temperature compensated. This difficulty might be overcome in practice by manufacturing a similar device out of a temperature independent material. To demonstrate the feasibility of such a device, however, PZT was utilized.

Chapter 2

EXPERIMENTAL PROCEDURE

2.1 Development of Procedure

2.1.1 Etching Rate Determination

In order to employ the microfabrication procedure, it was necessary to find a chemical etchant capable of dissolving PZT. A. P. Honess reports that almost any mineral can be etched using a combination of HCl, HNO_3, H_2SO_4, HF, NaOH, KOH, or a fused mixture of potassium bisulfate and powdered fluorspar (60). As many of the commercially available photoresists are developed in alkaline solutions (3), the hydroxides would probably strip off the polymer, making basic etchants incompatible with the patterning process. Consequently, a preliminary study on the efficacy of various acids in dissolving the ceramic was conducted.

Samples for etching studies were prepared by layering 30 2.8 mil tape cast sheets (prepared by TAM Ceramics Inc. from a PZT 501 powder) carrier side down and laminating in a warm press at 65^oC and 15,000 psi for one minute. Following a five-day binder burnout at 500^oC, the samples were fired in a lead-rich atmosphere with a four-hour ramp to 1285^oC and a one-hour soak. Any roughened or irregular edges were then smoothed by polishing with a coarse powder.

The resultant ceramic pellets were weighed to $\pm0.0002g$ using a Mettler AC100 balance and sized approximately (within $\pm0.2mm$) with a ruler. Each piece was then immersed in a beaker of concentrated acid maintained at temperature to within $\pm3^oC$ with a water bath and hot plate. After a specified time the sample was removed, rinsed, cleaned ultrasonically, rinsed again, dried under a flow of air, and reweighed (61-63). This process was repeated on a single disk until a constant slope of cumulative mass

loss per surface area per time was achieved. (See Fig. 14) The slope of the linear portion of the curve was then taken as the etching rate. Results of the preliminary investigation are given in Table 2.

A modified procedure was utilized for more accurate determinations of etching rates in the most promising acids. In this case, each sample was immersed in concentrated HCl at 45°C for five minutes both to clean the surfaces and to remove damaged areas (63). This in turn eliminated the non-linear portion of the etching curve usually attributed to either polished or defective surfaces (62), (64,65). Sample dimensions were determined with micrometers for calculations of nominal surface areas and densities.

The etching process was then carried out by holding the specimen in an acid bath maintained within ±0.5°C of a stated temperature for 60 seconds. After the allotted time had elapsed, the sample was washed immediately to remove any remaining acid, and then cleaned, dried, and weighed as previously. In all cases the surface area occluded by the tweezers was considered negligible. Results of this work are displayed in Table 3.

Etching of the ceramic with HCl was invariably accompanied by the formation of a whitish powder on the surface of the PZT, so that thorough ultrasonic cleaning was necessary to remove it from small crevices. X-ray diffraction identified this powder as pure PZT, suggesting that HCl etches by dissolving around the grains, rather than etching through them. Further support for this hypothesis is given in SEM micrographs of disks etched in HCl (Figs. 15,16) which display angular surfaces composed of whole grains and negligible rounding of individual grain apices.

Glassy, PbO-rich grain boundaries have previously been reported for certain PZT compositions (66). Consequently, it seems likely that the high etching rate of PZT in HCl is due to a preferential attack of the acid along the grain boundaries.

This mechanism has some important effects on the etching of the ceramic. In the first place, it leads to a rapid increase in the surface roughness of a disk which in turn can seed the formation of deep pits with prolonged etching. As this would be problematic
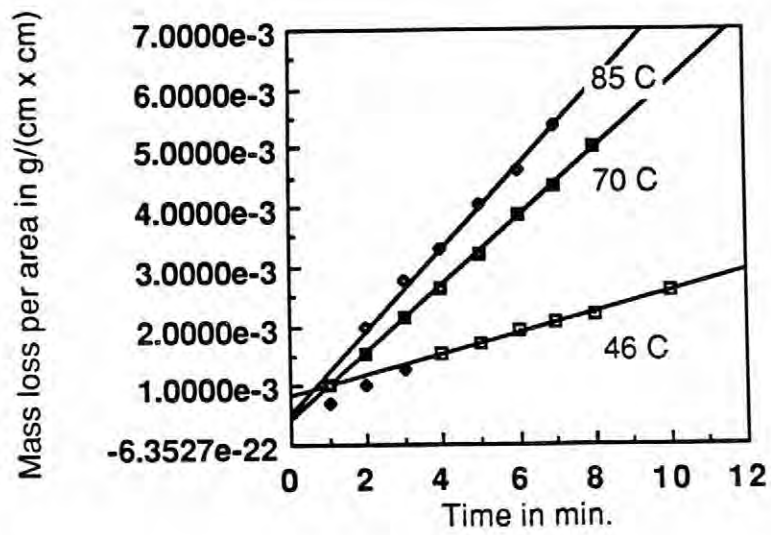
Fig. 14: Etching of PZT in H_3PO_4 at three different temperatures

Table 2: Preliminary data on the etching rate of PZT in various acids

Acid	Temperature (°C)	Etching rate $\left(\dfrac{g}{cm^2 \cdot min}\right)$
H_3PO_4	Room Temp.	9×10^{-5}
H_3PO_4	45-48	2×10^{-4}
H_3PO_4	61-65	2×10^{-4}
H_3PO_4	68-73	6×10^{-4}
H_3PO_4	82-88	7×10^{-4}
HNO_3	43-45	9×10^{-5}
HCl	42-48	4.5×10^{-3}
HCl	48-51	2×10^{-3}
H_2SO_4	42-48	3×10^{-4}
$0.5HCl - 0.5H_3PO_4$	49-50	3×10^{-4}
$0.25HCl - 0.75H_3PO_4$	49-51	4×10^{-4}

Table 3: Etching of PZT in HCl and aqua regia

Acid	Temperature (^oC)	Etching rate $\left(\dfrac{g}{cm^2 \cdot min}\right)$
HCl	30 ± 0.5	2.1×10^{-3}
HCl	45 ± 0.5	3.4×10^{-3}
HCl	60 ± 0.5	4.6×10^{-3}
$0.75HCl - 0.25HNO_3$	45 ± 0.5	9.7×10^{-4}
$0.75HCl - 0.25HNO_3$	60 ± 0.5	2.0×10^{-3}
$0.75HCl - 0.25HNO_3$	70 ± 0.5	3.6×10^{-3}
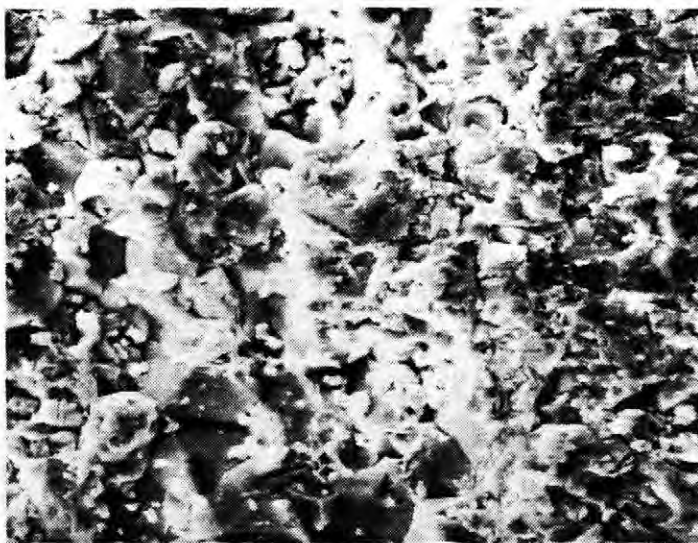
Fig. 15: Scanning electron micrograph of an unetched disk
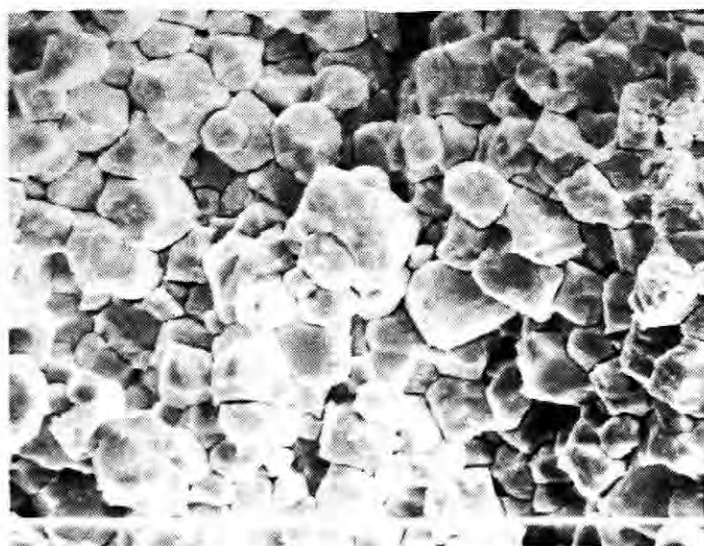
Fig. 16: Scanning electron micrograph of an etched PZT surface

during micromachining, it was avoided both by using thin samples and by maintaining a constant flow of acid over the surface of the wafer. Secondly, grain boundary etching should minimize the dependence of etching rate on the polarization direction noted by many authors in work on perovskites (20,21), (23). Thus, although all of the work in this study was performed on unpoled samples, it is expected to be applicable to poled specimens as well.

2.1.2 Photoresist

With this information it was then possible to find a compatible photoresist. Only two were tried, a G. C. Electronics Negative resist for circuitboards (G. C. Electronics, Rockford Illinois, 61101 USA) and Shipley S1400-27 Microposit positive resist (Shipley Company Inc., Newton Massachusetts, USA). The latter was chosen for further work both because it was designed to resist the attack of the most promising etchant, HCl (which the negative resist did not), and because it could be applied more reproducibly, leading to more accurate patterns. This choice did, however, impose some limitations on the etchant as HNO_3 and H_2SO_4 did cause the resist to peel up from surfaces. Consequently, the selection of this resist confirmed the use of warm concentrated HCl as the etchant.

As explained in section 1.2.1.1, positive resists contain a photoactive compound, a resin, and a solvent system. Although the exact composition of the Shipley resist utilized is proprietary, the company lists 2-ethoxyethyl acetate, butyl acetate, and xylene as the solvent base for their S1400 series resists (2).

In order to apply the resist, the ceramic was first cleaned with water and acetone, spun at high speed to remove dust, and then spun again after two-thirds of the surface had been covered with resist. This produced a very thin, even coating of the resist on the surface. Following coating, wafer and resist were pre-baked at 80°C for 20 minutes to remove the solvent.

Patterning of the resist was accomplished by exposing selected areas of the surface to intense white light. Using a rectangular array of four 300 to 375 watt bulbs, each approximately 27" from the sample, exposures of most designs could be made in 25 minutes. For very fine lines or for thicker resist coatings, however, exposure could take up to 40 minutes. Patterns were then developed by immersing the sample in a 1:1 solution of Microposit Developer CD-30 and deionized water and agitating lightly for 90 seconds. This stripped the resist from exposed areas. To further harden the resist after developing, patterned wafers were post-baked for a minimum of 20 minutes at $80^{\circ}C$.

The exact conditions of the patterning--spin speed, length of exposure, and baking times and temperatures--depended on both the device geometry and the severity of the etching conditions. It was found that a spin speed of 2000 rpm and a moderate post-bake ($80^{\circ}C$ for 50 minutes) produced a resist capable of withstanding HCl attack at $50^{\circ}C$ for over an hour, but which dissolved readily in an acetone bath after etching.

2.1.3 Photomasks

The photomasks used in this paper were 35mm film negatives prepared by photographing computer generated enlargements of the design. To attain the highest contrast between light and dark areas, both high contrast film and developer were employed. (Kodak Technipan film and D-19 developer) These photomasks were then placed on the resist coated wafer and held in place with a glass flat during exposure.

In those cases where both sides of a PZT wafer were to be patterned, an envelope of two photomasks was created by taping the negatives together. Alignment of the patterns was done by eye.

2.2 Optimized Processing Procedure

Wafers used in device manufacture were prepared from pellets made either by laminating tapes or pressing blanks. Slurries for tape-casting consisted of 35 weight percent Cerbind CB 73140 binder (Tam Ceramics Inc., San Marcos California, USA) and commercially prepared PZT 501 powder. This mixture was ball milled in a plastic jar for 16-17 hours with ZrO_2 media both to achieve homogeneity and to break up soft powder agglomerates. Before the mixture resettled, it was cast onto clean glass plates and air dried. (A schematic of the casting system is given in Fig. 17) Finished tapes were peeled away from the glass flats, punched into 1" square sections and laminated at 70°C, 7000 psi for three minutes. Binder was removed during a five-day binder burn-out cycle.

PZT powders for pressing pellets, on the other hand, were mixed with a 20 weight percent polyvinyl alcohol binder (7 grams binder to 100 grams PZT) dried, and ground until they passed through an 80 mesh sieve. Pellets were formed in a Carver press by pressing to 10,000 psi in steel dies. Once formed, these blanks underwent a binder burnout cycle consisting of a half-hour hold at 300°C, a half-hour ramp to 550°C, and then a one and a half hour hold at that temperature (67).

In both cases, burned out parts were loaded on to platinum sheets and fired with a PbO source using a five-hour ramp to 1285°C, a one-hour hold, and then slow cooling (67). Once sintered, samples were poled in a silicone oil bath at 110°C by subjecting them to a field intensity of 20 kV/cm for 12 minutes. This done, they were then polished to the desired thickness using a series of Al_2O_3 powders. Because the clarity of the photolithographic pattern was enhanced by smooth wafer surfaces, the final polishing was done with 3 μm grit.

Prior to applying the photoresist, the samples were spun for 20 seconds at 2000 rpm to remove dust. Then, working under yellow lights to prevent premature resist
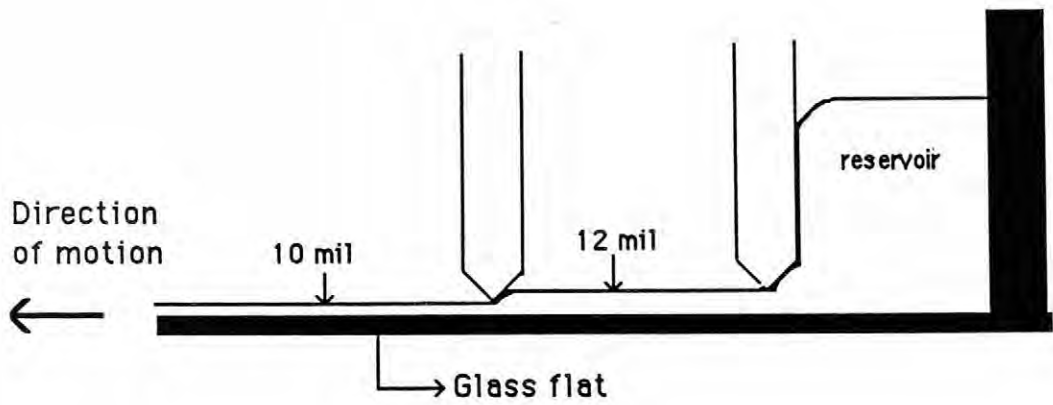
Fig. 17: Schematic of the tape casting system

exposure, enough resist was placed on the surface to cover 2/3 of the disk and the spin cycle was repeated. The second face was coated in a similar fashion. All samples were then placed in a light tight container and baked for 20 minutes at 80°C. The dried photo-resist was exposed under an array of white light bulbs for approximately 25 minutes using a photomask to delineate the pattern.

After exposure, the wafers were developed in a dilute Shipley Microposit Developer for 1.5 minutes to remove exposed areas. They were then post-baked, usually for 50 minutes at 80°C to further harden the remaining resist.

Following patterning, the disks were placed in a bath of warm concentrated HCl for etching. In order to remove reaction products from the surface and so present fresh acid to the cavities (1), it was necessary to agitate the liquid. An arrangement which proved adequate is pictured in Fig. 18. Once the pattern was completely etched, the piece was rinsed in distilled water and the resist was removed with a spray of acetone.

Electrodes were hand-painted on to device surfaces using an air-dry silver paint; any necessary electrical connections were then made by gluing silver wires to the sil-vered surface with a conducting epoxy.

It should be noted that the choice of a grain boundary specific etchant does impose some limitations on the device geometries which can be obtained with this technique. Trenches with openings only a few grain diameters wide would be difficult to etch and would probably be inhomogeneous (i.e. the sidewalls would not be smooth and straight but instead would follow grain contours). Given the fact that the devices in this study were on a much larger scale than the grain size (grain diameters of ~1-10 μm were observed in the scanning electron microscope), this microscopic heterogeneity was disregarded.

In the event that this technique were later to be applied to more miniature size scales, the rapid etching rate of HCl would not be as critical, and an etchant which was not specific to grain boundaries could be employed. The development of an anisotropic etchant for PZT similar to those used in silicon seems unlikely, however, as at present
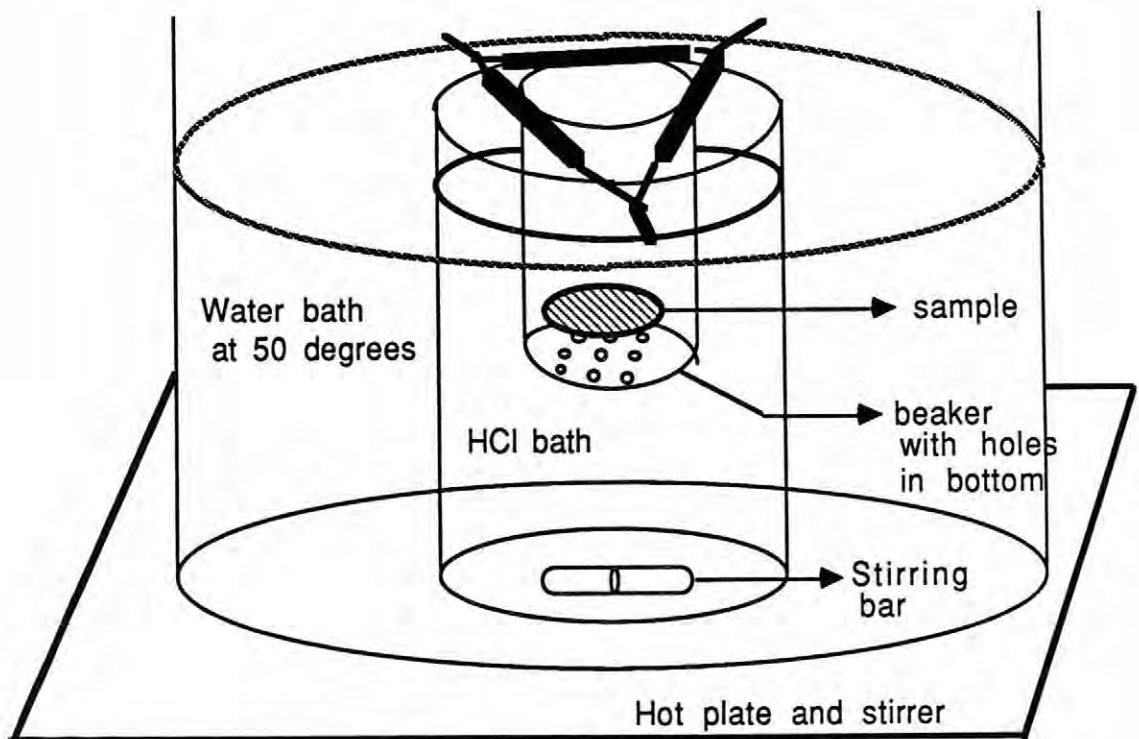
Fig. 18: Schematic of the etching system

attempts to grow single crystal PZT have been unsuccessful. Consequently, any chemical etchant chosen for use with small features would have to be isotropic and so would be constrained in turn to cavities twice as wide as they were deep (1). The more attractive alternative in this case would then be plasma or reactive ion etching.

Chapter 3

FLEXURAL MODE RESONATORS

3.1 Measurement Techniques

Resonance frequency data, including capacitance, conductance and impedance values, were collected using a Hewlett Packard 4192A LF Impedance Analyzer interfaced to a personal computer. Flexure mode "H" cantilever devices were suspended from the sample holder by wires affixed to the center bar so that they hung freely in air. These same wires also served as electrical connections, establishing the potentials illustrated in Fig. 10, page 17. In order to minimize hysteritic effects caused by subjecting a ferroelectric to large alternating fields, oscillation voltages of 0.1 Volts were utilized throughout these experiments.

Several flexural mode transducers are pictured in Fig. 19.

3.2 Resonance Characteristics

3.2.1 Fundamental Flexural Resonance

Representative examples of the first flexural resonance of "H" cantilever devices in air are given in Figs. 20-22. In general they demonstrate clean, sharp peaks with a Q_m of approximately 80-100 (highest value obtained was ~170), near the intrinsic value of PZT-5 (35). Occasionally, though, the resonance is split so that either distinct peaks (Fig. 23) or a shoulder (Fig. 24) appear. This occurence can be attributed to either slightly mismatched cantilevers (i.e. a gouge in one of the "H" legs) inhomogeneous electrode patterns, or similar imperfections. Details on the sizes of the resonators are given in Table 4.
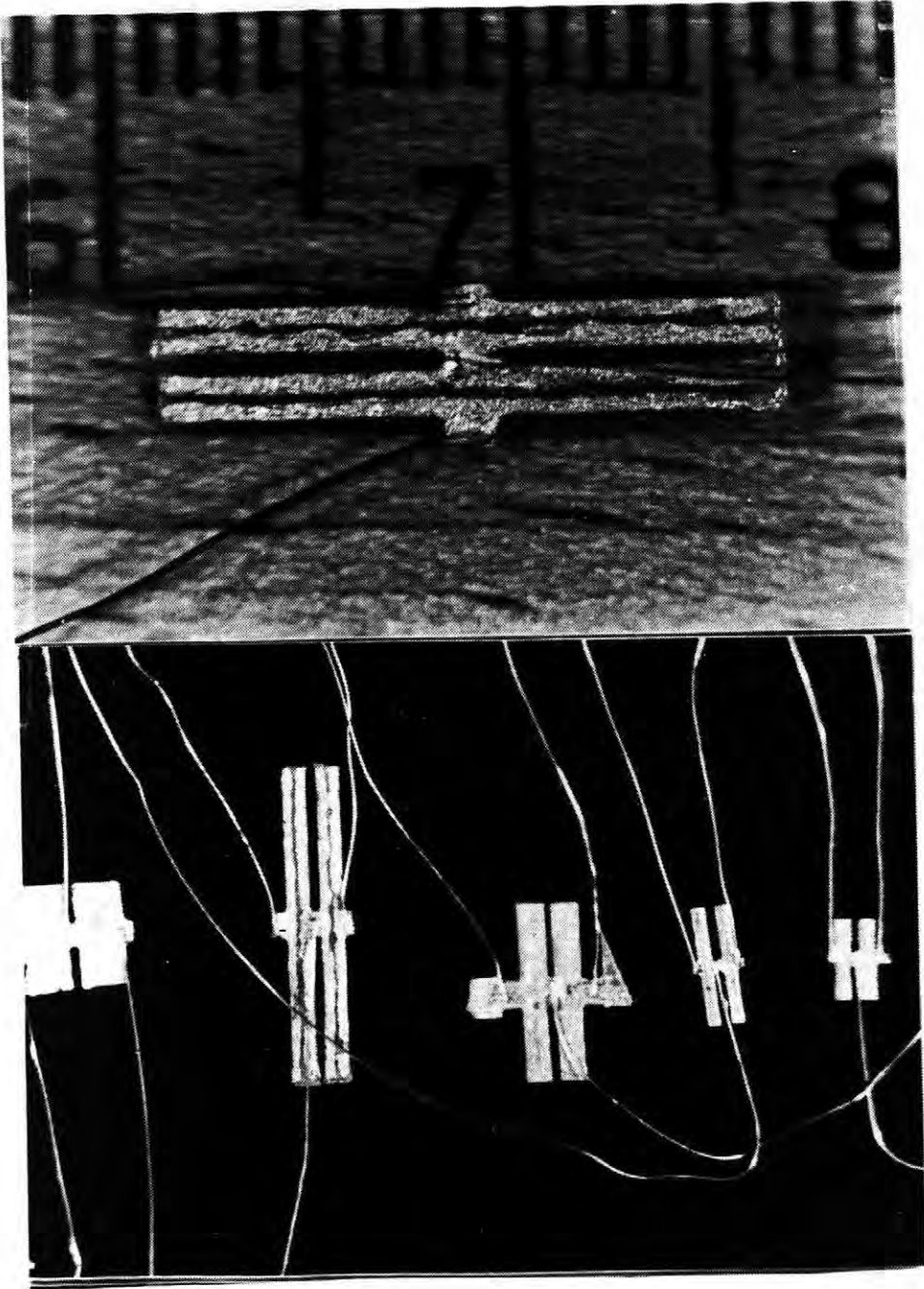
Fig. 19: Etched flexural mode transducers
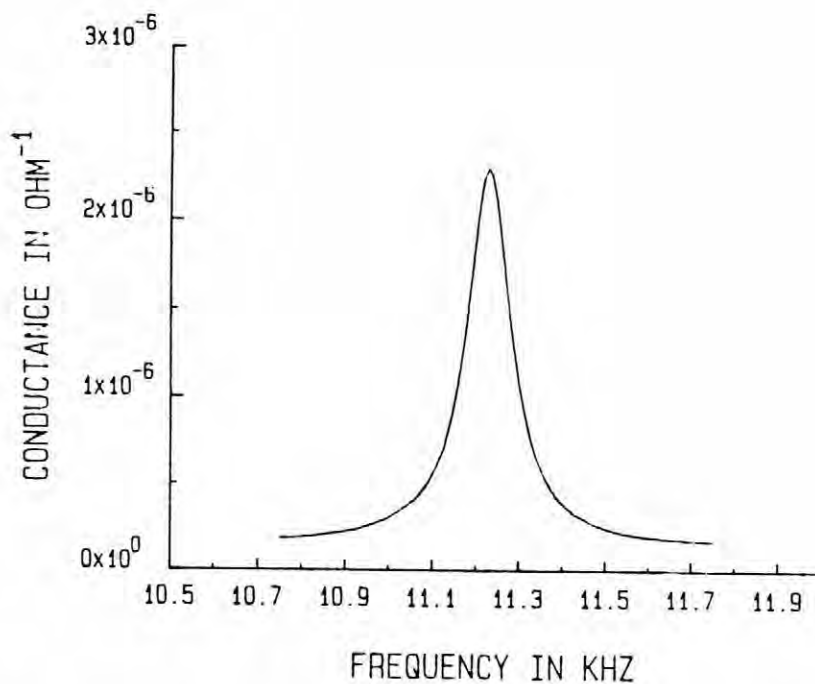
Fig. 20: Fundamental flexural resonance of an "H" transducer (See Table 4)
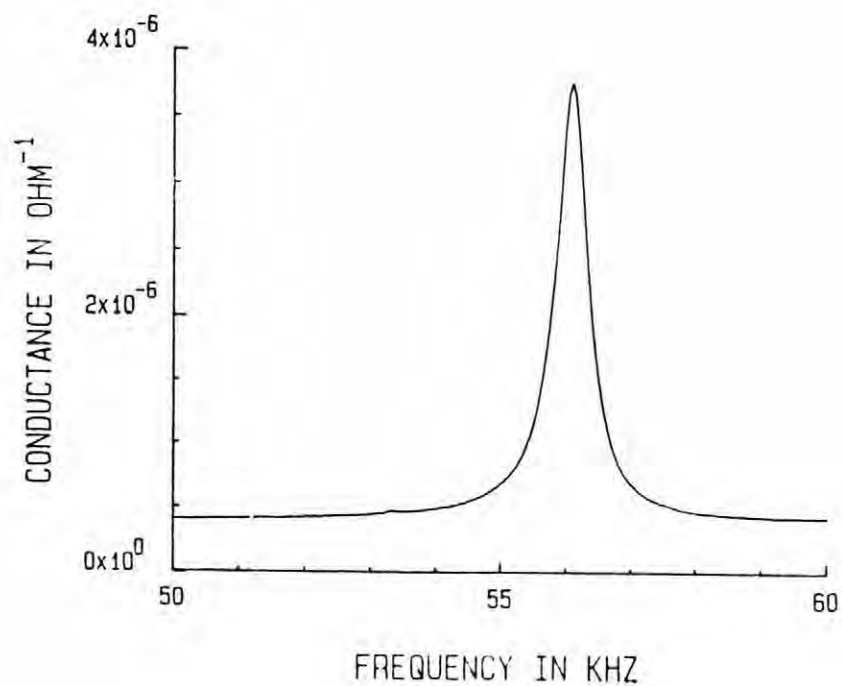
Fig. 21: Fundamental flexural resonance of an "H" transducer (See Table 4)
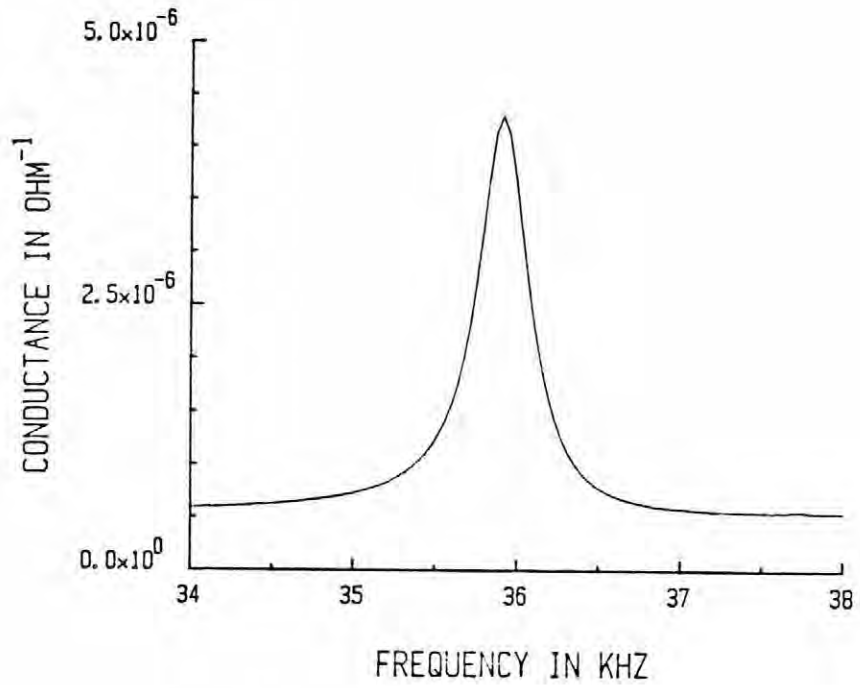
Fig. 22: Fundamental flexural resonance of an "H" transducer (See Table 4)
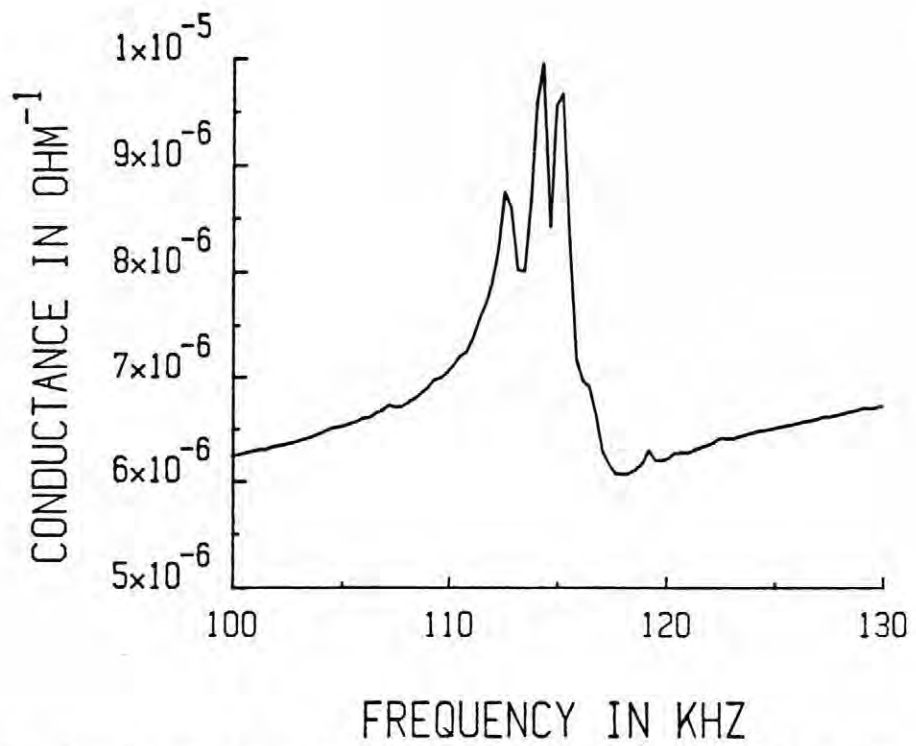
Fig. 23: Split fundamental flexural resonance of an "H" transducer caused by poor

electrode patterning (See Table 4)
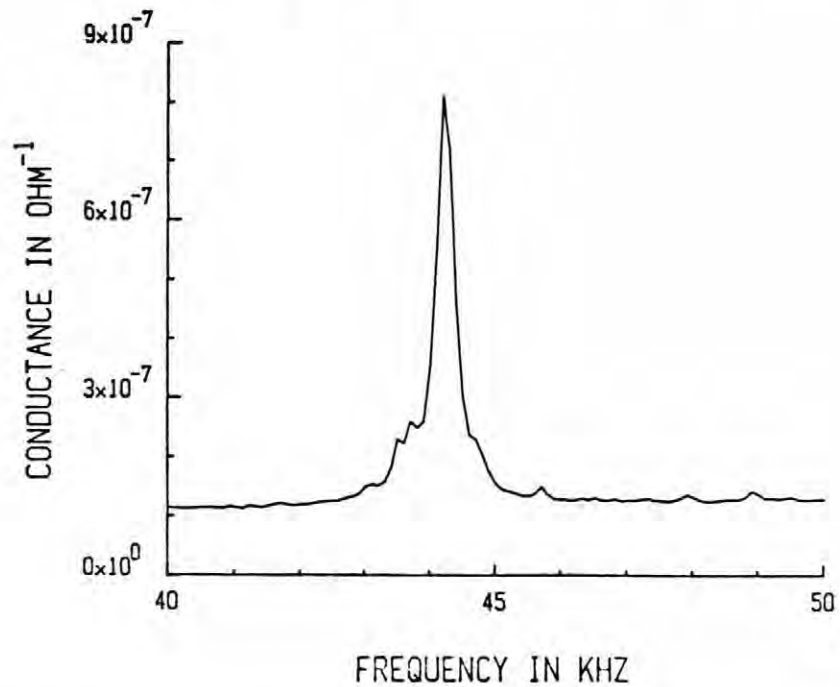
Fig. 24: Fundamental flexural resonance of an "H" transducer showing shoulder on peak

(SeeTable 4)

Table 4: Geometry and resonance behavior for the resonators in Figs. 20-24

Fig.	Cantilever length	Cantilever width	f_r in kHz Exper.	f_r in kHz Calc.	Q_m
20	7mm	1mm	11.23	~9.5	94
21	3mm	1.2mm	56.32	~62	94
22	3.5mm	1.2mm	35.96	~45	100
23	2mm	2.5mm	~115	~290	----
24	~2.6mm	0.75mm	44.20	~52	~110

The frequency range over which fundamental flexural resonances were generated was 10 to 115 kHz, as determined by the sample geometry. In general, those cantilevers which were long in comparison to the width generated low frequencies; shorter or wider bars were responsible for the upper end of the frequency spectrum. Although the Euler beam formula did approximate the placement of the resonances, it proved increasingly inaccurate at the higher frequencies where the cantilevers could no longer be properly treated as thin bars (See Table 4). The resultant shear and torsion terms dropped the resonance frequency below the predicted value.

The exact placement of the resonance frequency for a single sample varied somewhat with the quantity of paint and epoxy used. Consequently, on re-electroding a transducer with a fundamental resonance at approximately 30 kHz, the absolute location could vary by up to a few kHz. However, once an oscillator was electroded, its resonance characteristics were stable over time. Thus, it should be possible to trim the electrodes on these resonators to precisely tune the resonance frequency, as is done for quartz tuning forks.

As expected from PZT, the transducers have temperature dependent properties. From measurements on a resonator mounted in a heated chamber, it was apparent that in addition to a slight shift in the resonance frequency, there was a significant broadening of the peaks as the temperature increased. This would be important in implementing these devices as density or viscosity meters and could require separate calibrations of the transducer for different temperature regimes.

3.2.2 Additional Resonances

To further characterize the properties of "H" transducers, scans of conductance versus frequency were made for frequencies above the fundamental flexural resonance. For reference, data were taken for a transducer of identical dimensions which had been completely electroded on both faces to eliminate the flexural response. The first length

resonance, for example, would be calculated from

$$f_r = \frac{nv}{2l}$$

with n = 1 (68) using the combined lengths of two collinear cantilevers and the center bar for l. Higher order length modes are given as integral multiples of the fundamental in Table 5.

The scans for a transducer with split electrodes were then compared to the fully electroded counterpart (See Figs. 25-29). As expected, the flexural resonances dominate the trace at low frequencies. At somewhat higher frequencies, the length vibrations correspond moderately well to the predicted values, though they are greatly reduced in amplitude.

All of these results for higher frequency resonances are somewhat dependent on the precision of the electroding.

3.3 Density Meter

3.3.1 Experimental Procedure

A listing of the liquids used in density and viscosity measurements is given in Table 6. Nominal densities of these liquids were determined by weighing a known volume of each. Restrictions on their compositions imposed by the experiment precluded the use of either conducting liquids (as these would short-circuit the device) or liquids like acetone which dissolved the silver paint. Plastic vessels were used throughout to minimize reflection of acoustic waves from container walls as those might detrimentally affect the experiment. Although initially all measurements were made on 50ml quantities of the liquids, some questions concerning fulfillment of assumptions in the theory (see section 3.3.3) prompted use of quart containers.

Table 5: Theoretical and experimental values for the length resonances of a fully electroded "H" transducer.

Calculated	Experimental
$f_1 = 167$ kHz	160 kHz
$f_2 = 335$ kHz	330 kHz
	420 kHz
$f_3 = 503$ kHz	540 kHz
$f_4 = 670$ kHz	590 kHz
$f_5 = 838$ kHz	835 kHz
$f_6 = 1005$ kHz	1000 kHz
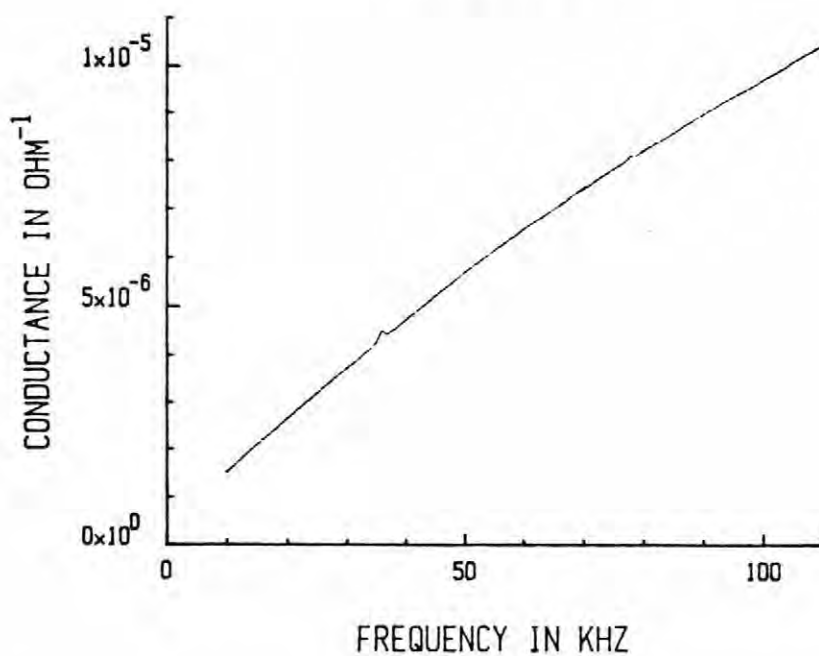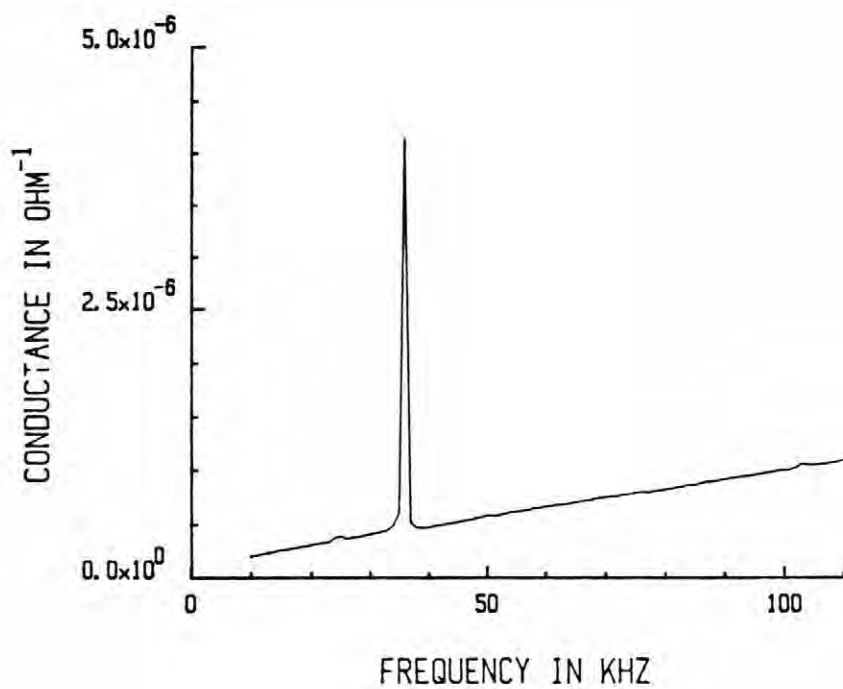
Fig. 25: Scans for partially (top) and fully (bottom) electroded "H" transducers:

0-100kHz
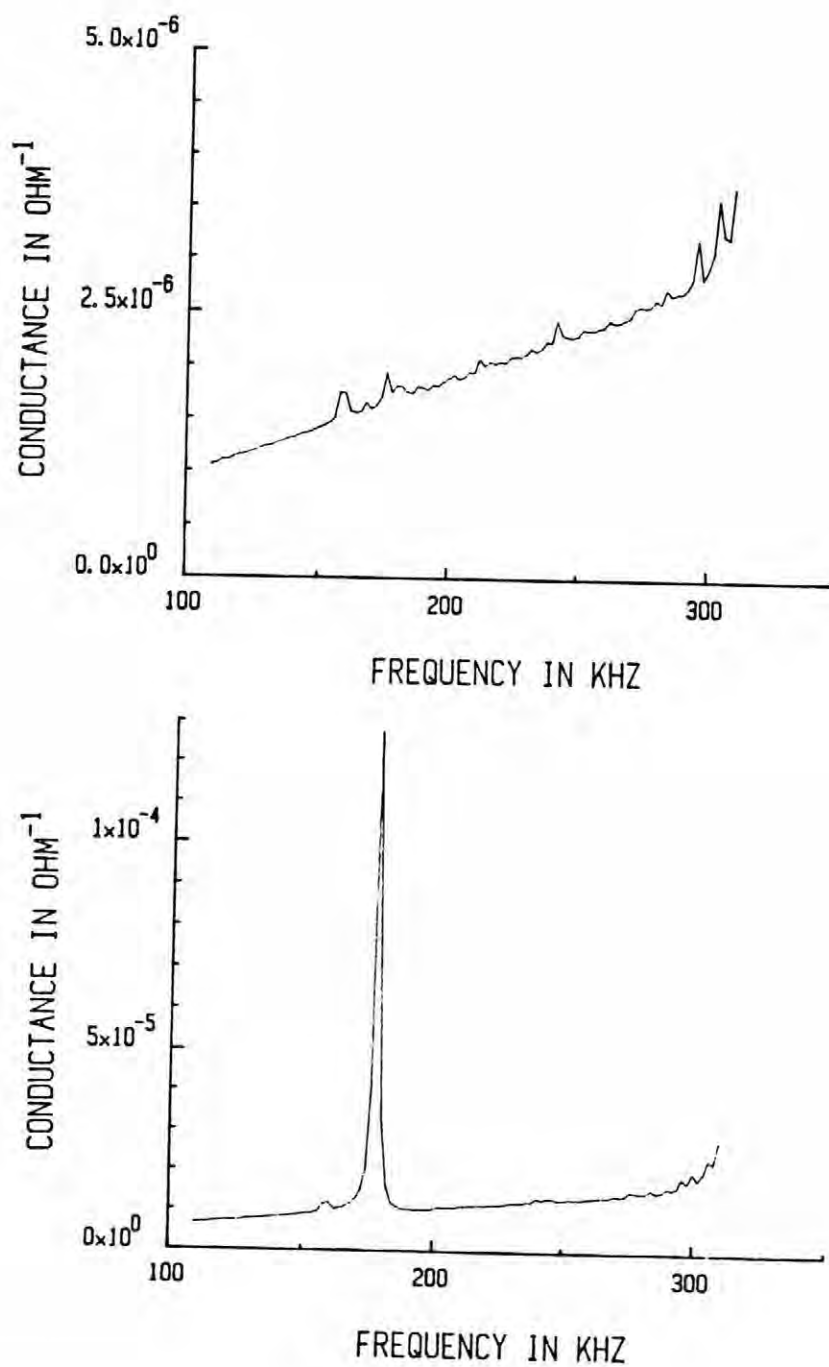
Fig. 26: Scans for partially (top) and fully (bottom) electroded "H" transducers: 100-300kHz
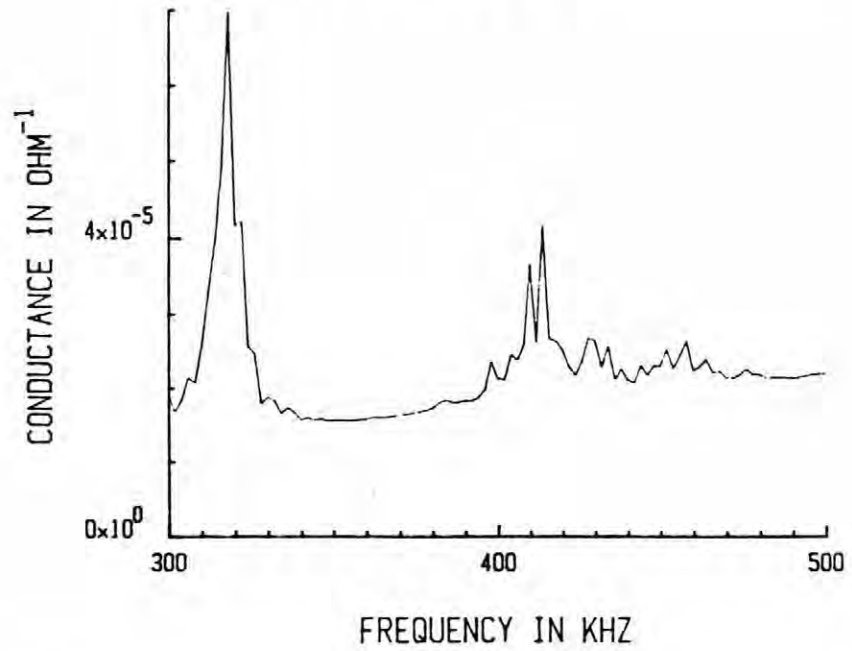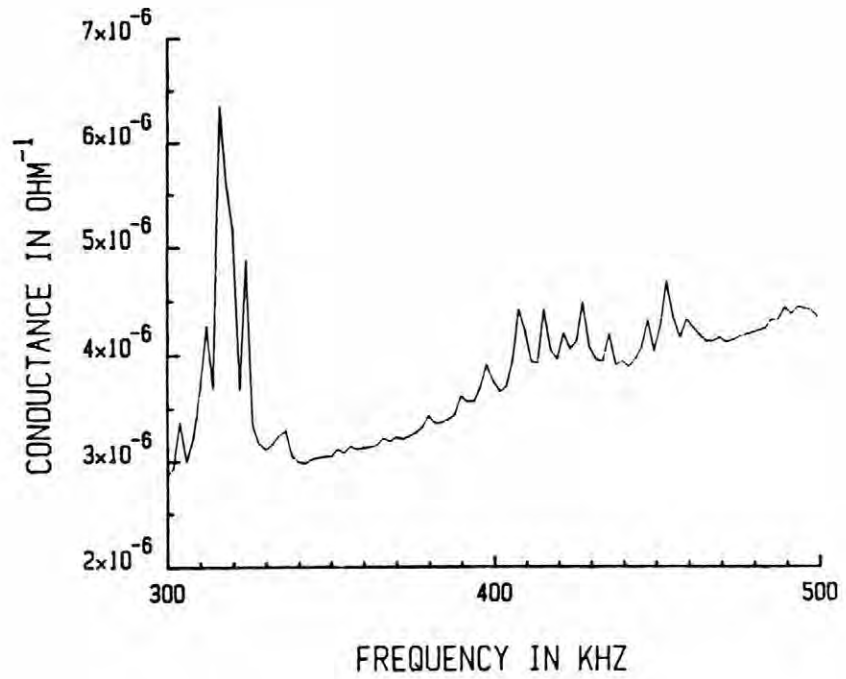
Fig. 27: Scans for partially (top) and fully (bottom) electroded "H" transducers: 300-500kHz
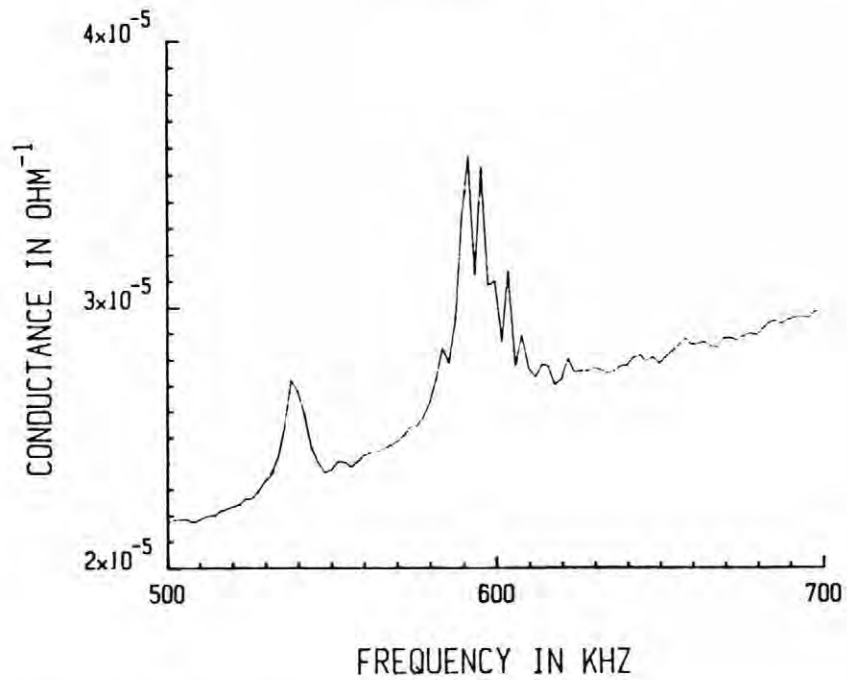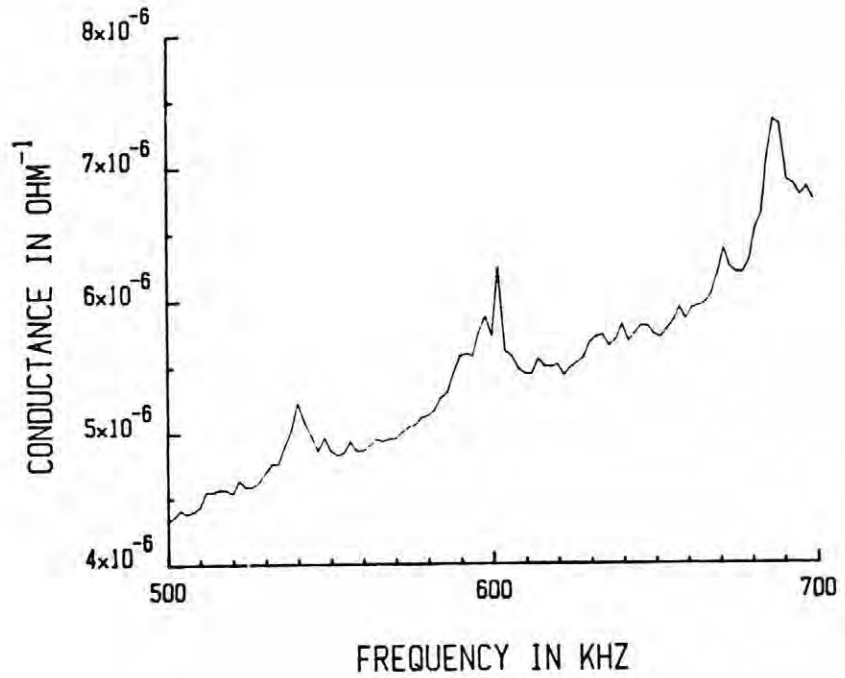
Fig. 28: Scans for partially (top) and fully (bottom) electroded "H" transducers: 500-700kHz

56
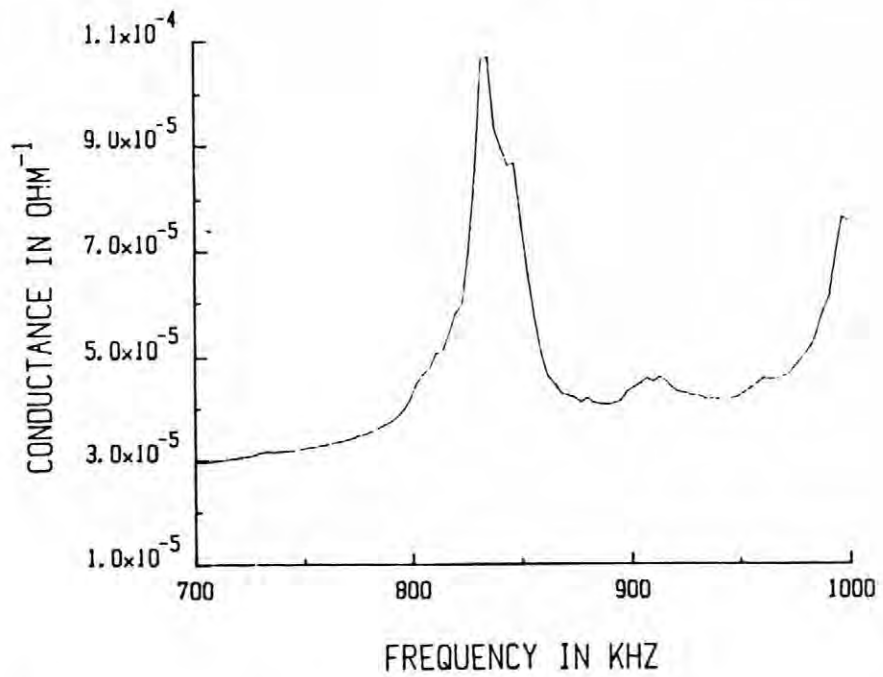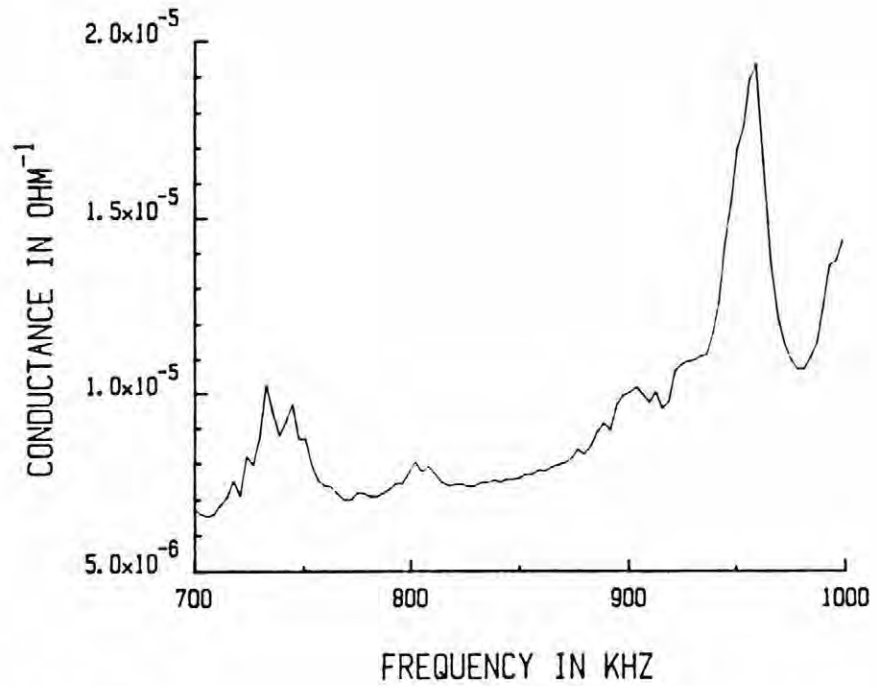
Fig. 29: Scans for partially (top) and fully (bottom) electroded "H" transducers:
700-1000kHz

Table 6. Liquids employed in density and viscosity measurements

---

Al Cass Valve Oil	Automatic Transmission Fluid
Corn Oil	DC 200 Silicone Oil
Deionized water	Extra Heavy Mineral Oil
Glycerin	Hydraulic Fluid
Hydraulic Jack Oil	Light Mineral Oil
Roche Thomas Valve Oil	SAE 20 Motor Oil
SAE 30 Motor Oil	

For density and viscosity measurements, samples were mounted in a holder, immersed in the liquid, and driven through the resonant frequency. After the data had been collected, the resonator was removed from the bath, rinsed in dishwashing detergent to remove excess oil, sprayed with deionized water, and dried. When the resonance in air had settled back to a given frequency, the next oil was examined. It was found that a thin coating of oil on the transducer improved the wettability of the device, preventing entrapment of air bubbles on the ceramic surface. Such bubbles would otherwise detract from the reliabilty of measurements as they create a region of effective low density and low viscosity on the transducer face.

During measurement, the "H" was completely submerged and held vertically near the center of the oil-filled beaker. Since the peak shift also depended on the depth of the transducer when it was located too near the surface, efforts were made to insure approximately a centimeter of liquid between the PZT and the air-oil interface.

3.3.2 Relation Between Peak Shift and Density

As predicted by the theory (section 1.3.1.3) vibrating an "H" transducer in liquids of disparate densities caused marked changes in the resonant frequency. Fig. 30, for example illustrates the appearance of the conductance versus frequency curves resultant when one transducer was vibrated in, from right to left, air ($\rho \sim 0 \ ^g/_{cm}3$), Al Cass Valve Oil ($\rho = 0.77 \ ^g/_{cm}3$), corn oil ($\rho = 0.91 \ ^g/_{cm}3$), and extra heavy mineral oil ($\rho = 0.88\text{-}0.89 \ ^g/_{cm}3$). From this it is apparent that as the density of the liquid increased, so did the shift of the resonance frequency from the value in air. This trend is further illuminated in Figs. 31-33, where f_r^{-2} is plotted as a function of the density. Error bars given for the y axis data points arise from the fact that peak broadening (see section 3.4.2) obscured the exact resonance frequency. Within these limits, however, the data points were reproducible.
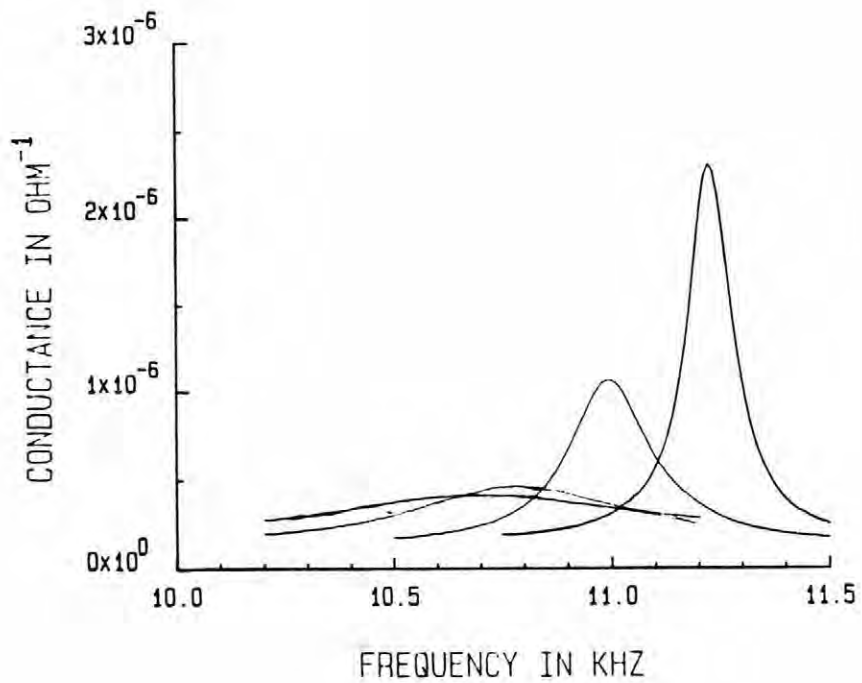
Fig. 30: Variation in resonance peak for vibration of transducer in different fluids [From right to left, air ($\rho \sim 0$ $^g/_{cm}3$), Al Cass Valve Oil (ρ=0.77 $^g/_{cm}3$), corn oil ($\rho = 0.91^g/_{cm}3$), and extra heavy mineral oil ($\rho = 0.88$-0.89 $^g/_{cm}3$).]

Fig. 31: Relation between resonant frequency and density for 18.8 kHz hard PZT transducer with dimensions of 1cm x 2mm x 0.2mm
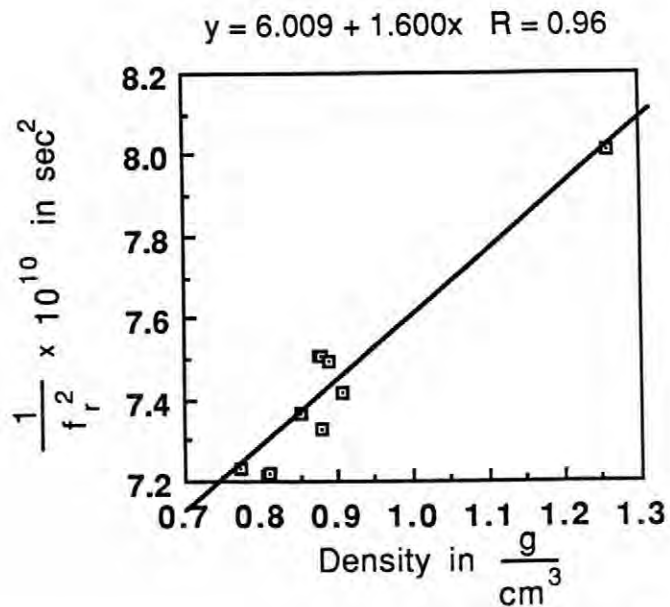
Fig. 32: Relation between resonant frequency and density for 37 kHz soft PZT transducer with dimensions of 6mm x 2mm x 0.2mm
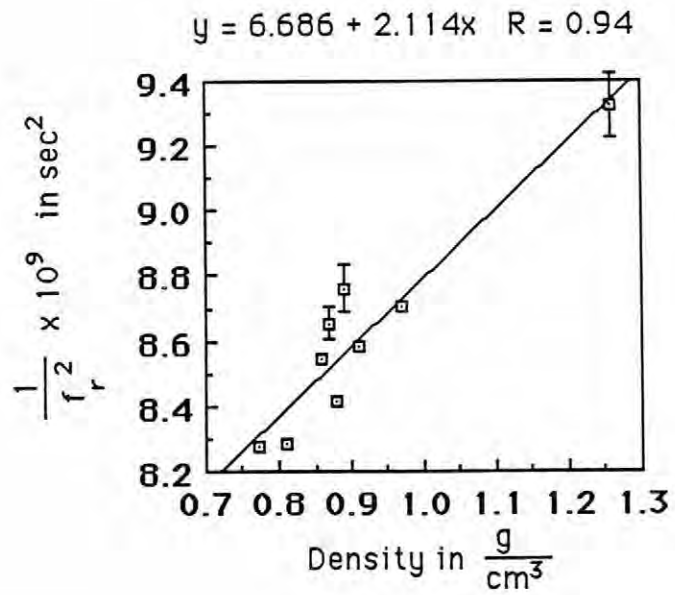
Fig. 33: Relation between resonant frequency and density for a ~10 kHz soft PZT

transducer with dimensions of 2cm x 2.5mm x 0.2mm

The graphs in Figs. 31 and 32 illustrate a good fit to the predicted linear correlation between f_r^{-2} and the density. It should be noted, however, that the least squares fits to the lines (given immediately above the graphs) do not extrapolate to the resonant frequency of the device in air, implying that the meter would be applicable only above some lower density limit. It was also found that measurements taken with ~18.8 and ~37 kHz transducers were more accurate than those derived from transducers oscillating at 10 kHz.

Despite the adherence of most of the points to the prediction, it is also clear that some of the data, particularly that taken at 10 kHz, deviate significantly from the line. Potential causes for this behavior are numerous. For example, moderate electrical conductivity caused peaks to shift too far below the readings in air, while high conductivity caused peaks to shift rapidly and erratically with time. This problem could easily be eliminated by coating the transducer with a thin layer of compliant plastic to electrically insulate it. Attempts of this kind were made, but it was difficult to attain a truly impermeable layer of Eccogel-0. Waterproofing of parts is, however, common industrially and would probably not constitute a major obstacle. A second problem which could prove more insidious results from the fact that the theory assumes that the transducer is a point source radiating into an infinite medium. This imposes several restraints on the sizes of both transducer and container and is considered more thoroughly in section 3.3.3.

Another possibility which was not explored, but which could prove interesting, is the behavior of the transducer in a solids-loaded liquid. If it could accurately measure the density of the mixture, and particularly if it simultaneously determined the viscosity (section 3.4), the device could find widespread use in the characterization of slurries.

3.3.3 Potential Geometric Limitations

The theory which predicts a linear change in f_r^{-2} as a function of density is derived for a point acoustic source radiating into an infinite medium. Practically, this implies
1) the resonator size should be much smaller than the wavelength of sound in the medium: size $<< \frac{1}{6}\lambda$.
2) the resonator should be surrounded with 2-3 wavelengths of liquid on all sides.

It is the first restriction which makes thickness mode transducers unlikely candidates for density meters as for a 1 MHz transducer vibrating in a liquid with $v = 1500$ $^m/_s$, the maximum permitted dimension would be 0.25mm. Similarly, low frequency oscillators are eliminated due to the secondary requirement; a one kHz transducer operating in the same liquid as above would require 380 m^3 of that liquid for an accurate measurement.

Unfortunately, it also proved difficult to simultaneously satisfy both conditions in the case of flexural mode resonators. Although the 10 kHz transducer with cantilever dimensions of 7.5mm x 1.5mm did just fulfill the size requirement, the quantities of liquid used in measurement were far too small, particularly in those cases where v approached 2000 $^m/_s$. This could account for the fact that better data was obtained for transducers with higher frequencies.

There are two potential means of sidestepping this problem. The first is to manufacture a transducer which approximately fulfills the requirements for a wide range of acoustic velocities (900-2000 $^m/_s$). This would probably require a transducer with an intermediate frequency (i.e. 40-50 kHz) which had a maximum dimension near 4.5mm. Preliminary attempts were made to fabricate a resonator with these specifications, but the bars were too thin to permit painting the split electrodes by hand. A second method by which these conflicting restraints could be circumvented is to utilize a series of transducers, each of which fulfils both requirements for a limited range of acoustic velocities.

3.4 Viscometer

3.4.1 Experimental Procedure

The experimental procedure for viscosity measurements was identical to that detailed in section 3.3.1. To monitor the peak width as a function of viscosity, plots of capacitance versus frequency were examined and frequencies f_1 and f_2, the maximum and minimum capacitance values respectively, were determined to the nearest 0.01 kHz. The difference f_2 - f_1 was then used as the peak width at half height. Reference viscosities, used as "true" viscosity values for each liquid were determined using a Brookfield model LVF Viscometer.

3.4.2 Relation Between Viscosity and Peak Width

Fig. 30, page 59, illustrates the variations in peak shape when a transducer is excited in media of different viscosities. From right to left, the scans representing air (η ~ 0 cp)(69), Al Cass Valve Oil (η ~ 1 cp), corn oil (η ~ 77 cp), and extra heavy mineral oil (η ~ 148 cp) demonstrate the expected increase in peak width as a function of viscosity. This observation is reaffirmed by the data in Figs. 34 and 35 which show the two to be proportional. It is interesting to note that for Fig. 34, the least squares fit to the line does not extrapolate correctly to the value obtained for Δf in air ($\Delta f = 0.036$ kHz in air) Consequently, since a knee in the curve must appear at some viscosity, it is not surprising that values for η ~ 1-2 cp (black diamonds) do not fit the curve. Above this cut-off, however, the device seems to be at least as reproducible as the Brookfield viscometer. Again, data taken at ~18.8 and ~37 kHz was more accurate than that derived from a 10 kHz transducer. (See Fig. 36.)
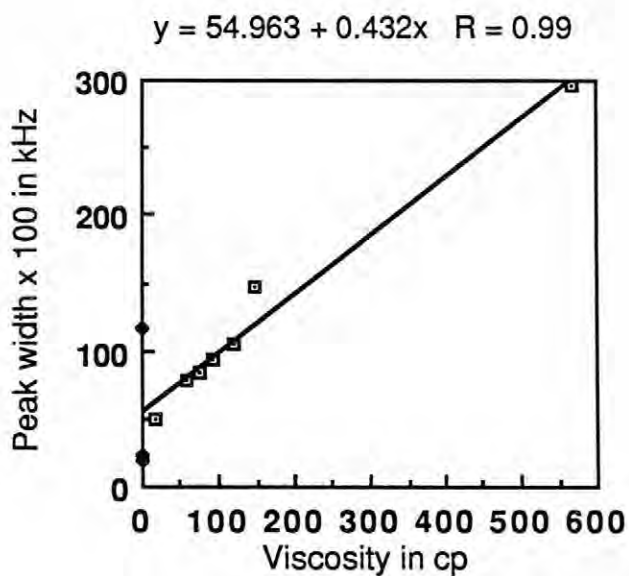
Fig. 34: Relation between peak width and viscosity for 18.8 kHz hard PZT transducer

with dimensions of 1cm x 2mm x 0.2 mm
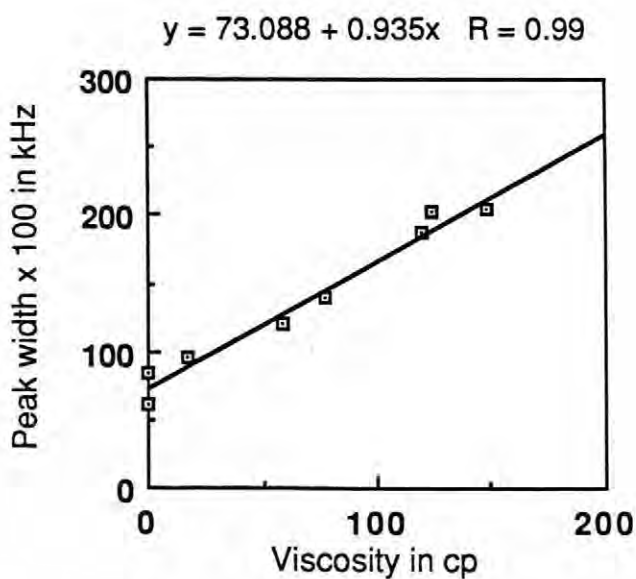
Fig. 35: Relation between peak width and viscosity for a 37kHz soft PZT transducer with

dimensions of 6mm x 2mm x 0.2mm
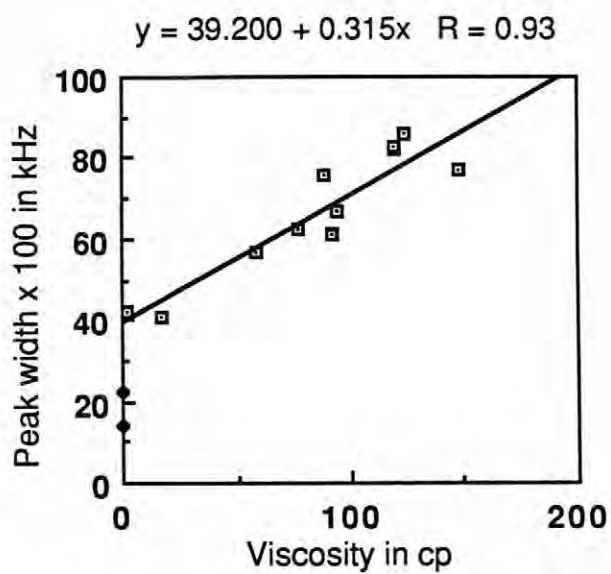
Fig. 36: Relation between peak width and viscosity for 10 kHz soft PZT transducer with dimensions of 2cm x 2.5mm x 0.2mm

In order to evaluate the potential applications for this type of viscometer, a more complete characterization of its properties should be undertaken. One of the most important of these would be the effect of container size on the accuracy of the measurements. If the "H" type transducer could operate effectively in a few drops of solution, it might find widespread use in areas like thick film ink manufacture where the liquids are both very expensive and available only in small quantities.

Another area in which piezoelectric viscometers could prove useful is in monitoring the shear rate dependence of viscosity. Utilizing a combination of flexural mode and other higher frequency shear wave oscillators, it would be possible to plot the percentage change in Q_m as a function of the resonant frequency. The behavior of the resulting curve might indicate transitions between relaxation mechanisms.

Chapter 4

THICKNESS MODE RESONATORS

4.1 Experimental Procedure

The equipment used to analyze the resonance behavior of thickness mode transducers is analogous to that described in section 3.1 for flexural devices. In this case, samples were thin (0.2 mm) disks of PZT with a diameter of ~1.6 cm; both faces were completely electroded with an air-dry silver paint. Electrical connections were made by lightly clamping the alligator jaws of HP test fixture 16407A on the center of the disk. Again, an oscillating voltage of 0.1 V was used for excitation to circumvent appearance of hysteritic effects. In order to measure planar coupling coefficients, resonant, f_r, and anti-resonant, f_a, frequencies were determined by locating the maxima in the conductance and resistance versus frequency curves respectively.

4.2 Relation Between Etching of Disks and Frequency Spectra

As explained in section 1.3.2, thickness extensional disk transducers with good planar coupling undergo radial resonances in addition to the thickness vibration when excited by an alternating voltage applied across the faces. The first five of these radial resonances appear in Fig. 37 as strong peaks in scans of conductance versus frequency. These resonances contrast strongly with the data of of Fig. 38 which shows the same frequency range for a transducer of identical dimensions which had been etched with a spiral extending from the center to 0.77r (See Fig. 39). Here it is seen that the first radial resonance, the one which had appeared at ~140kHz, has been completely destroyed. Similarly, the great disparity in scales for the two plots demonstrates that remaining
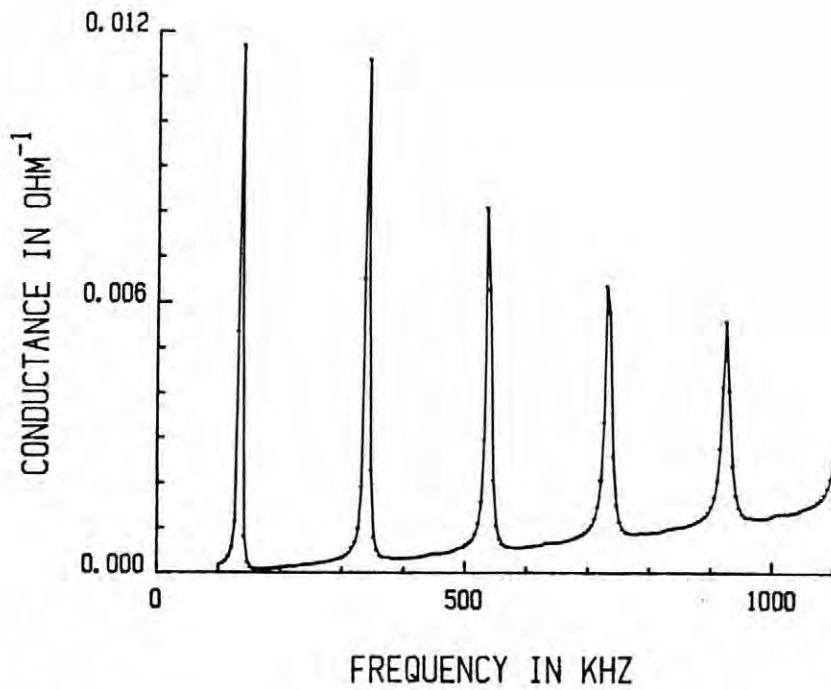
Fig. 37: Radial resonances of a disk transducer
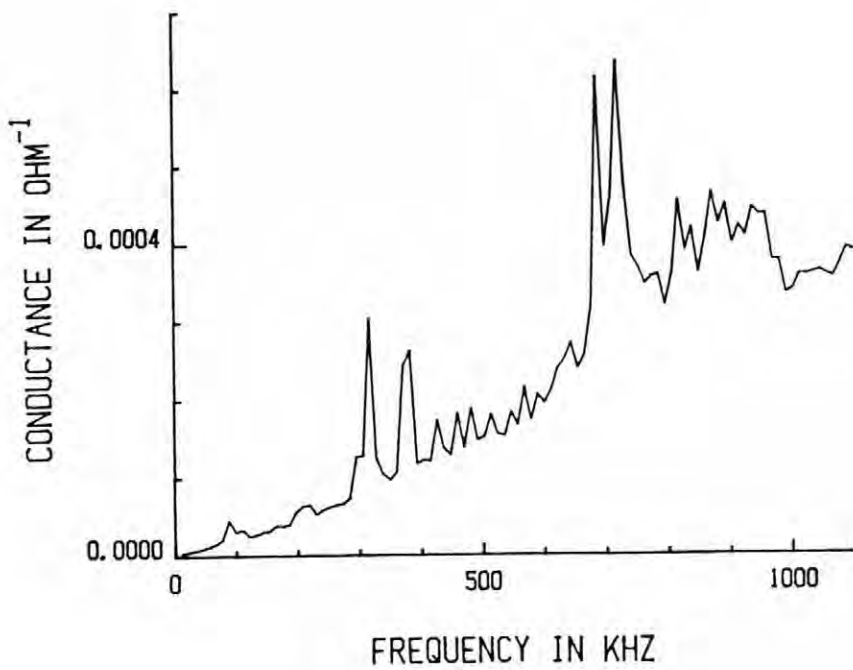
Fig. 38: Frequency scan of a modified disk transducer showing decreased lateral

resonances
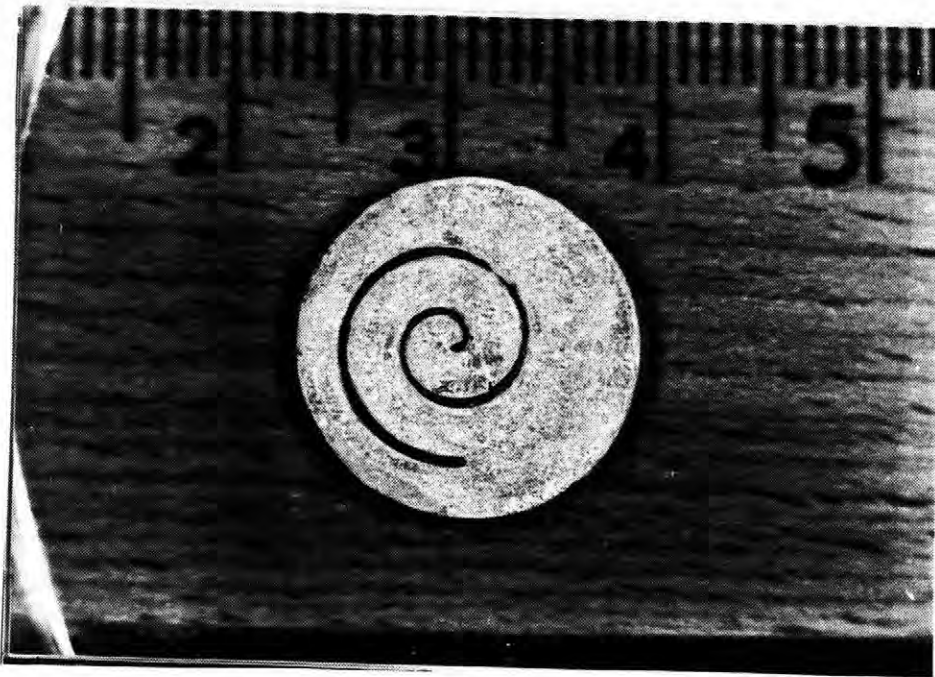
Fig. 39: Photograph of an etched disk transducer

resonances have also been drastically reduced in amplitude. Thus it is clear that the patterning effectively disrupted several of the primary radial resonances.

As a result of the etching, the planar coupling coefficient for the disk decreased to 0.06, where k_p was calculated from

$$k^2_{eff} = \frac{f^2_a - f^2_r}{f^2_a}$$

(49) since the modified transducer did not possess a simple geometry. Unfortunately, there were no isolated peaks due to lateral vibration modes, so it was necessary to use peaks separated by only 14 kHz for the calculation. Although this implies that the absolute value obtained for k_p is not accurate, it does illustrate a marked reduction in planar coupling from the reported value if 0.63 (35).

This ability to selectively destroy unwanted resonances could have a significant impact on transducer fabrication. Elimination of radial resonances in a disk transducer, for example, would forestall the need for replacement of PZT parts with $PbTiO_3$, permitting retention of the higher thickness coupling coefficients found in PZT. The result would be an acoustic imaging system of the same resolution with more efficient conversion of electrical to mechanical energy. In addition, the higher dielectric constant of PZT ceramics leads to better compatibility with the electrical impedance of the accompanying electronics (53). It is also interesting to note that the processing technique is better suited to thin disks because progressively narrower linewidths can be etched as the etched depth decreases. Thus, unlike the case of the PZT/polymer 1-3 composites (See section 1.3.2.1), these transducers would probably be easier to manufacture as the resonance frequency of the disk increased. Consequently, the two resonator types could serve in complementary frequency regimes with the transition between the two occurring at $\sim$ 1-5 MHz.

Chapter 5

DELAY LINE DEVICES

5.1 Experimental Procedure

Measurements of the time required for acoustic waves to propagate down the length of a PZT spiral involved comparing a reference pulse to signals taken from various points along the sample as shown in Fig. 40. Each shaded area shown was mirrored on the converse side by an identical electrode; wires were attached to both faces so that one surface could be grounded and the other linked to the input of an oscilloscope. Ten- to thirty-volt signals from an HP 214B Pulse Generator were then simultaneously pulsed into channel A of a Tektronix, Inc., Type 545 Oscilloscope and the center electrode on the spiral at a frequency of 1kHz. Unamplified delayed waves were detected as voltage pulses on the second channel of the oscilloscope.

5.2 Results

Fig. 41 pictures two ceramic spirals produced by chemically etching PZT. Particularly in the case of the smaller of the two, the fine features were more easily obtained by patterning both sides of the disk and permitting etching through both faces. In this way, overetching of the thin PZT bars did not occur.

Photographs of typical delayed signals are given in Figs. 42-44 where the top scan represents the input pulse and the bottom the response from the piezoelectric. In all cases, the output was clearly visible with the oscilloscope set to register 0.05 volts per cm division. Data on the delay times achieved to date appear in Table 7. These values prove that a compact piezoelectric delay line is possible.
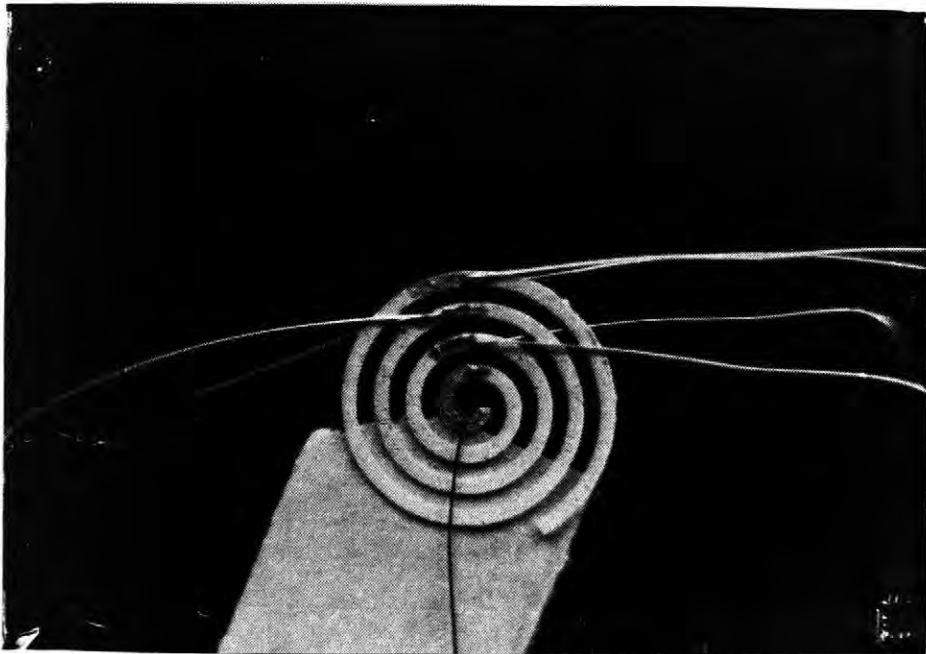
Fig. 40: Sample for delay line measurements
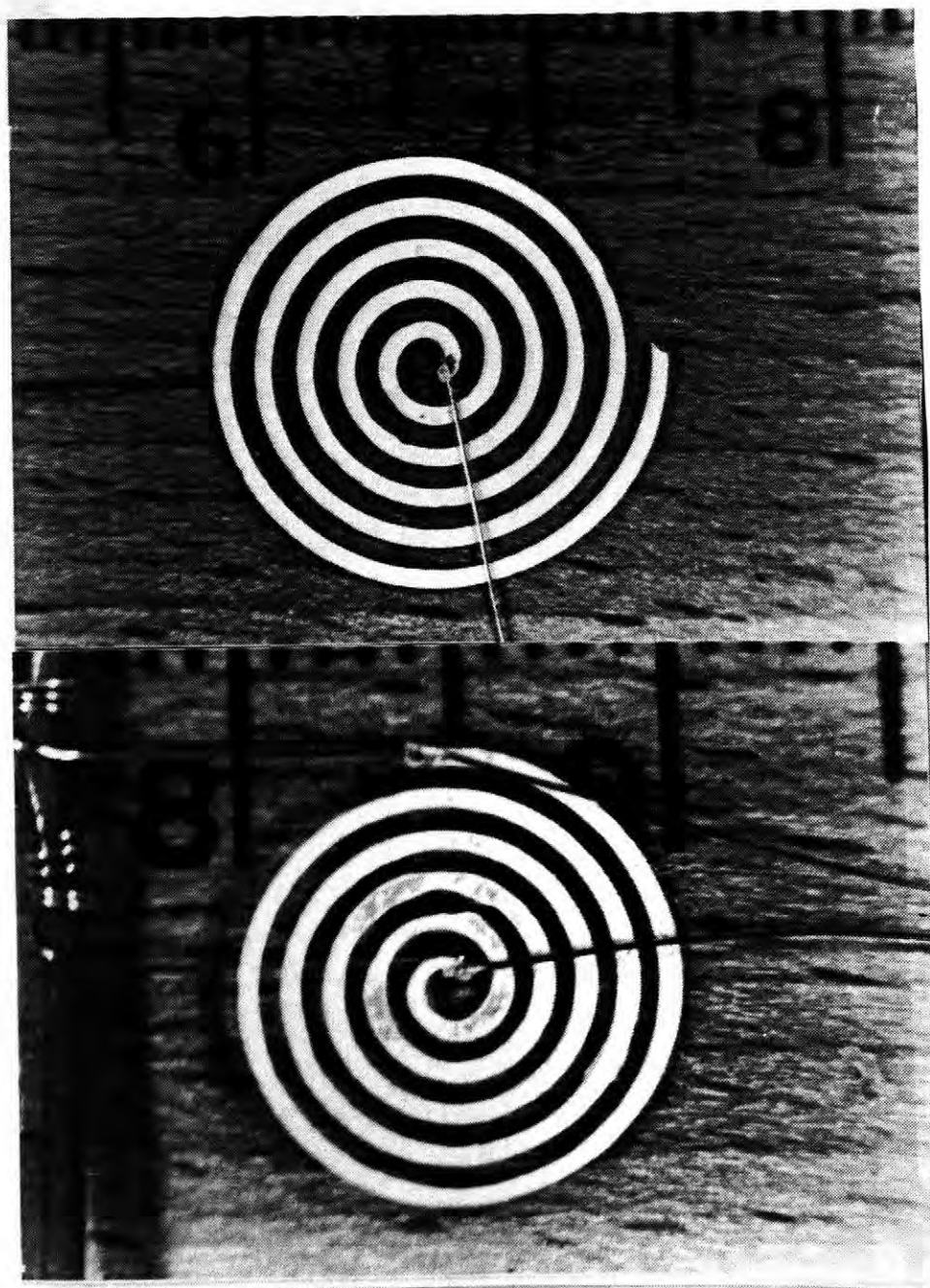
Fig. 41: Etched piezoelectric delay lines (numbered divisions in cm)

75
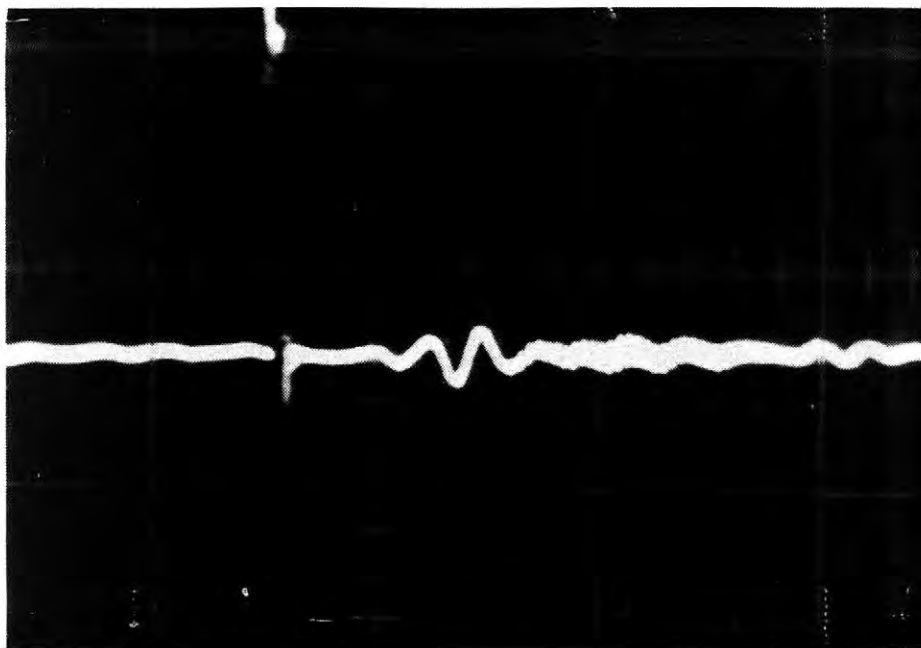
Fig. 42: Ten μs delay (x axis = 10μs per div., y axis = 0.05V per div.)
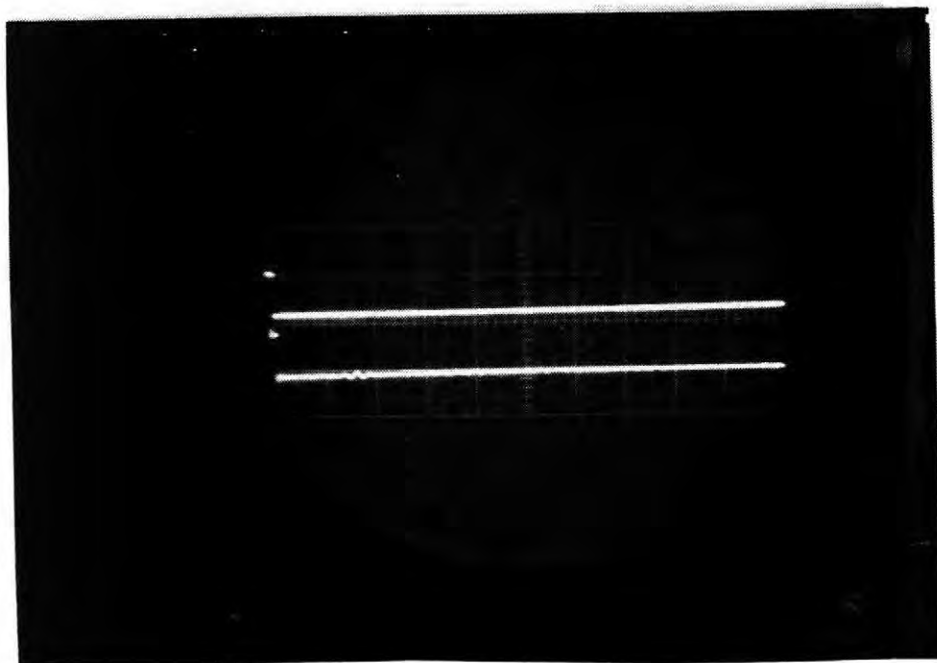
Fig. 43: Eighteen μs delay (x axis = 10μs per div., for top scan y axis = 20V per div.,

bottom scan y axis = 0.05V per div.)
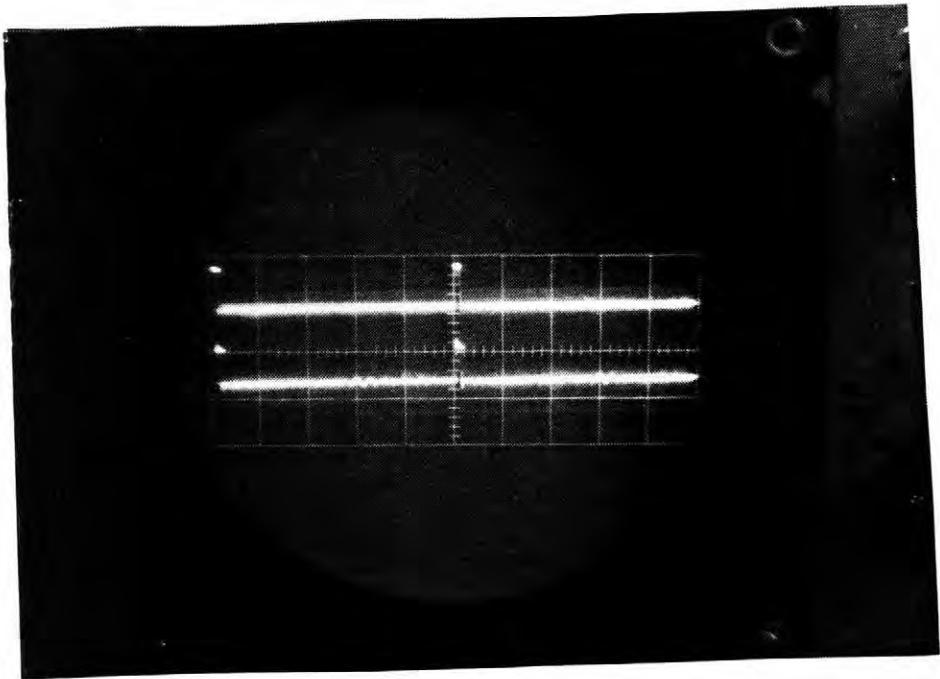
Fig. 44: Thirty μs delay (x axis = 10μs per div., for top scan, y axis = 20V per div.,

bottom scan, y axis = 0.05V per div.)

Table 7: Experimentally determined delay times from PZT spiral

Delay time	Input Signal	Output Signal
10μs	20V	0.02V
18μs	20V	0.0125V
30μs	20V	0.01V

The absolute shape of such a delay line would probably be tailored to minimize distortion of the pulse, and might not be a spiral as shown here. In conjunction with this, it would probably be necessary to hot press the ceramic disks to prevent reflections from pores from interfering with the signal.

It should also be noted that these samples would be very difficult to fabricate by any other processing method. Consequently, it seems clear that this technique could broaden the range of available devices by expanding the spectrum of accessible sample geometries.

Chapter 6

CONCLUSIONS

6.1 <u>Discussion</u>

This thesis has proved that photolithography and chemical etching can be applied successfully to the production of piezoelectric devices. The degree by which it will be adopted industrially is dependent both on the evolution of new device types which would be difficult to reproduce by other methods and the extent to which it eases fabrication of existing ones.

As there is no fundamental limitation on the length and width dimensions of the piezoelectric sheet to be patterned, this technique should be well suited to the production of device arrays. Unlike the dicing methods commonly employed today, it would require neither the individual devices nor the array itself to be rectilinear or regular. In the third dimension, the thickness is limited by the time required to etch cavities of the desired depth. Most of the devices investigated in this work, for example, were completed after one to one and a half hours of etching in concentrated HCl. Although this time could probably be decreased by addition of fluoride ions to the etchant, it would still remain a significant portion of the processing time for thick specimens. Consequently, it is likely that the technique would be applied primarily to thin (<< 1mm) samples.

An additional problem imposed by thick samples is the constraints subsequently imposed on the lateral dimensions of any device. Because many of the ferroelectrics with good properties, most notably those located near morphotropic phase boundaries in multi-component systems, cannot be grown as single crystals, micromachining is limited to the use of isotropic or grain-boundary etchants. This in turn implies that any etched cavity will be twice as wide as it is deep. Thus, Brodie and Muray (1) suggest that

the minimum feature size patterned on a film which is to be etched completely through should be three times the film thickness.

This last restriction can, however, be relieved somewhat by a number of methods. For example, it is possible, as was done in this thesis, to pattern both sides of the substrate and etch through both faces into the middle. It is also believed that aspect ratios of slightly better than 1:2 were achieved using a grain-boundary specific etchant, perhaps because the agitation was more efficient in removing grains from the bottom than the sidewalls of a trench. This effect could be exploited by spraying the acid at the substrate during etching to dislodge grains as they were loosened.

Even with these improvements though, it is clear that the processing procedure is more appropriate for thin samples and small feature sizes. Indeed, it is the extremely fine device sizes that can be produced which sets photolithography apart from other techniques. Resolution of $< 2\mu m$ is common today in microelectronics. Although this investigation was confined to macroscopic devices, it would be interesting to see comparable size scales appear in ceramic substrates perhaps through the use of a dry etching process like sputter or reactive ion etching.

Another significant advantage this technique displays over more conventional methods is the fact that the processing is comparable to that used in integrated circuit manufacture. Consequently, it appears that these devices would be amenable to integration with semiconductor electronics. This in turn could make production of miniature piezoelectric devices and sensors feasible.

6.2 Summary

This work has demonstrated that the coupling of photolithography with chemical etching is a viable processing technique for ceramic materials. The method is readily

adapted to a variety of two-dimensional patterns and is particularly suited to small feature sizes.

For a PZT 501 substrate, warm, concentrated hydrochloric acid was found to be a grain-boundary specific etchant with a comparatively rapid etching rate. As several commercial photoresists, notably Shipley S1400-27, were able to withstand the attack of the acid for periods of greater than one hour, it was chosen for all micromachining studies.

PZT disks fabricated by conventional techniques were prepared for patterning by polishing with $3\mu m$ grit and spin-coating the photoresist onto the wafer. After soft-baking to remove the solvent, the resist was exposed through a high contrast 35mm film negative patterned with the negative image of the final device. Wafers were then developed, post-baked, and etched to transfer the design to the PZT.

Using this technique, several small piezoelectric devices were prepared from thin ($\sim 0.2mm$ thick) ceramic disks. Among these were flexural resonators, thickness extensional resonators, and acoustic delay lines.

The flexural mode transducers consisted of four cantilevers arranged around a center bar so that the device looked like a capital "H." By varying the geometry, fundamental resonances between 10 and 115 kHz could be generated. The electronic properties of these devices were measured to analyze both the fundamental and higher order resonances.

An "H" transducer was then used as a density meter by tracking the change in the resonant frequency during vibrations in different liquids. Plots of f_r^{-2} versus ρ were linear for the density range of $\sim 0.78 - 1.3$ $g/_{cm}3$. Nevertheless, there are some outstanding questions concerning the sizes of the resonator and the fluid bath required for the most accurate operation of the meter.

Measurement of the viscosity of the fluid medium could also be made with an "H" transducer. It was found that due to the attenuation of sound radiated into the liquid, the

peak width decreased in direct proportion to the viscosity. The device appeared to be similar in accuracy to the Brookfield viscometer used for calibration. If this accuracy is retained in particle-loaded liquids, such a transducer could be valuable in the character-ization in slurries and thick film inks.

Micromachining was also used to destroy the symmetry of thickness extensional disk transducers in order to reduce coupling to the lateral resonances. By etching a thin spi-ral through the thickness of the disk, the planar coupling coefficient was reduced to ~0.06 for a PZT specimen. This could make manufacture of high frequency (>2 MHz) PZT transducers for medical imaging systems possible.

The last device explored was an ultrasonic delay line. In this case, a planar spiral etched from a PZT wafer was used both to convert pulsed signals between electrical and mechanical energy and to propagate the acoustic wave. As several taps could be spaced along the length of the spiral, this configuration could serve as a variable delay line. For commercial application of this device, it would be necessary to design the system to minimize pulse distortion.

It can be concluded from this work that micromachining of miniature piezoelectric devices is possible using photolithography and chemical etching. Several devices were produced which would be difficult to replicate using other processing methods, suggesting that the technique should expand the types of geometries available to device designers. Moreover, as the process is not materials specific, it can be applied to a wide range of substrate wafers.

6.3 Future Work

Although it is known that a bound exists on the minimum device size which can be obtained using a grain boundary specific etchant, no attempt was made to determine it in the etching of PZT with HCl. Both this and an estimation of the aspect ratio, (depth of

trench)/(width of opening), which can be attained would be crucial in delimiting the size scale on which piezoelectric devices could be made.

Further characterization of the devices described in this thesis should also be undertaken. Both the density and the viscosity meters, for example, would be most useful if they operated accurately in solids-loaded liquids. Consequently, the determination of the transducer's behavior in such liquids could be essential to their implementation in industry. It would also be interesting to check the validity of the assumption that the viscosity of the fluid does not alter the peak position by repeating the experiment with a tuning fork with higher Q_m.

Investigations on the reduction of the planar coupling coefficients for modified disk transducers were conducted only on the resonator itself. To fully evaluate the properties of such a transducer and its value to medical imaging then, it would be necessary to add backing and impedance matching layers so that it could be incorporated into a working system. In this way, studies of the interference of lateral modes with the thickness resonance could pinpoint the optimum etching pattern.

The etching of thickness mode disk transducers could also be extremely useful in the production of annular ring transducers. These systems require a number of concentric rings of equal area and are desirable because they permit focussing in 2 directions, a significant advantage over conventional transducers. Unfortunately they are also difficult to fabricate. Using the process described in this thesis, however, production of such resonators could be comparatively easy. One path which could be pursued would involve embedding a PZT disk in epoxy and polishing one face until the ceramic was exposed. This could then be patterned and etched in the usual fashion with the epoxy preventing etching on the opposite face. The trenches could then be backfilled with a polymer, and the back face of the transducer polished to reveal the etched regions. Electroding of the faces could then be accomplished using the usual techniques.

Another area which would be interesting to explore is the production of miniature bimorphs from a ceramic wafer bonded to a metal shim. This would permit flexure to occur perpendicular to the plane of the device. Such a configuration would be extremely useful as a pressure sensor or accelerometer. Preliminary experiments along this vein suggest that two etching steps would be necessary because of the disparity in etching rates between the ceramic and the metal plate. Thus, the metal would probably be etched first in dilute acid and then completely covered with a resist during etching of the ceramic. Without this additional step, etching of the metal is so rapid that the resist peels off.

Either a bimorph or an "H" transducer could then be mounted flush to the side of an object immersed in a fluid undergoing turbulent flow. Pressure induced flexure of the cantilevers would result in the appearance of a voltage in the piezoelectric which could be monitored. If an array of very fine elements were used in this way an accurate measurement of the pressures involved in near field turbulence can be made.

REFERENCES

(1) Ivor Brodie and Julius J. Muray. The Physics of Microfabrication, New York: Plenum Press 1982.

(2) Shipley product literature on Microposit S1400 Series Photoresist and Microposit Developers, Newton Mass., 1985.

(3) David J. Elliot. Integrated Circuit Fabrication Technology. New York: McGraw-Hill Book Company, 1982.

(4) King, "Future Developments for 1:1 Projection Photolithography," IEEE Trans. Electron Devices ED-26(4) p. 711 (1979).

(5) J. H. Bruning, "Performance Limits in 1:1 UV Projection Lithography," J. Vac. Sci. Technol. 16 p. 1925 (1979).

(6) H. I. Smith, D. L. Spears and S. E. Bernacki, "X-ray Lithography: a Complementary Technique to Electron-Beam Lithography," J. Vac. Sci. Technol. 10(6) p. 913-917 (1973).

(7) Pedro Lilienfeld, "The Defocussing Barrier: an Optical Shield Against Particle Contamination," Microcontamination 4(10) p. 36 (1986).

(8) Marjorie K. Balazs, "A Summary of New Methods for Measuring Contaminants in Ultrapure Water," Microcontamination 5(1) p. 34 (1987).

(9) Roger K. Lachenbruch and Octavio Gomez, "Control of Particulate Emissions From Plasma Etching Systems," Microcontamination 5(1) p. 42 (1987).

(10) Kenneth E. Bean, "Anisotropic Etching of Silicon," IEEE Trans. Electron Devices ED-25 (10) p. 1185 (1978).

(11) David Wang and Jerry Wong, "Etched Trenches Conserve Semiconductor Device Space," Vacuum Technology p. 107-112 (1985).

(12) Susumu Takahashi, Fumio Murai, Hiroshi Kodera, "Submicrometer Gate Fabrication of GaAs MESFET by Plasma Etching," IEEE Trans. Electron Devices ED-25(10) p. 1213 (1978).

(13) James B. Angell, Stephen C. Terry, and Philip W. Barth, "Silicon Micromechanical Devices," Scientific American (April 1983).

(14) Ernest Bassous, "Fabrication of Novel Three-Dimensional Microstructures by the Anisotropic Etching of (100) and (110) Silicon, " IEEE Trans. Electron Devices ED-25(10) pp. 1178-1185 (1978).

(15) Eduard A. Gerber and Arthur Ballato Eds. Precision Frequency Control. New York: Academic Press Inc., (Harcourt Brace Jovanovich, Publishers) 1985.

(16) Eishi Momosaki and Shigeru Kogure, "The Application of Piezoelectricity to Watches," Ferroelectrics 40 pp. 203-216 (1982).

(17) T. Shiosaki and A. Kawabata, "Machining of PZT, PT, and (Mn, Zn) Fe_2O_4 Ceramics by Laser-Induced Chemical Etching," Third U.S.-Japan Seminar on Dielectric and Piezoelectric Ceramics Programs and Abstracts 1986.

(18) Tadashi Shiosaki, Mataoki Tanizawa, Hidenori Kamei, and Akira Kawabata, "Laser Micromachining of a Modified $PbTiO_3$ Ceramics in KOH Water Solution," J. Appl. Phys. 22 Supplement 22-2 pp. 109-112 (1983).

(19) H. Silcock, Ed. Solubilities of Organic and Inorganic Compounds. New York: Pergamon Press (1979).

(20) G. L. Pearson and W. L. Feldman, "Powder Pattern Techniques for Delineating Ferroelectric Domain Structures," J. Phys. Chem. Sol. 9 pp. 28-30 (1958).

(21) D. S. Campbell and D. J. Stirland, "A Modified Replica Technique and its Application to the Examination of Etched Single Crystals of Barium Titanate," Brit. J. Appl. Phys. 7 pp. 62-65 (1956).

(22) V. J. Tennery and F. R. Anderson, "Examination of the Surface and Domain Structures in Ceramic Barium Titanate," J. Appl. Phys. 29 pp. 755 (1958).

(23) J. A. Hooton and W. J. Merz, "Etch Patterns and Ferroelectric Domains in $BaTiO_3$ Single Crystals," Phys. Rev. 98(2) pp. 409-413 (1955).

(24) E. P. Guenok, Yu. V. Zabara, A. Yu. Kudzin, and O. I. Formichev, "Investigation of the Fine Structure of Barium Titanate Crystals," Soviet Physics -- Solid State 12(3) pp. 751-752 (1970).

(25) G. V. Belekopytov et. al., "Dielectric Nonlinearity of Single Crystal Strontium Titanate," Soviet Physics -- Solid State 23(1) pp. 79-84 (1981).

(26) Fumiko Hayashi, Yutaka Hayashi, and James D. Meindl,"Chemical Etching of Piezo-electric Ceramics," Chemical Abstracts 86: 94832, Chemical Abstracts Service, Columbus, Ohio.

(27) T. I. Bakunova et. al., "Etchant for Lead Zirconate Titanate Ferroelectric Ceramic," USSR patent SU 988,854 Chemical Abstracts 98: 118085, Chemical Abstracts Service, Columbus, Ohio.

(28) G. H. Haertling, "Improved Hot-Pressed Electrooptic Ceramics in the (Pb,La)(Zr,Ti)O$_3$ System," J. Am. Cer. Soc.54(6) pp. 303-309 (1971).

(29) Hiroshi Takeuchi and Shigeru Jyomura, "Tuning Fork Resonator Using Modified PbTiO$_3$ Ceramics," Appl. Phys. Lett. 37(10) pp. 891-893 (1980).

(30) William T. Thomson. Theory of Vibrations With Applications. Englewood Cliffs, New Jersey: Prentice-Hall Inc., 1972.

(31) J. F. Nye. Physical Properties of Crystals. New York: Oxford University Press, 1985.

(32) Michael A. Marcus, "Performance Characteristics of Piezoelectric Polymer Flexure Mode Devices," Ferroelectrics 57 pp. 203-220 (1984).

(33) Turukevere Ramarao Gururaja. Piezoelectric Composite Materials for Ultrasonic Transducer Applications. Ph.D. thesis, Pennsylvania State University (1984).

(34) Lawrence E. Kinsler and Austin R. Frey. Fundamentals of Acoustics. New York: John Wiley and Sons, Inc., 1962.

(35) Product Literature of Piezokinetics Inc., Bellefonte, Pa.

(36) Robert Resnik and David Halliday. Physics Part 1 Third ed. New York: John Wiley and Sons, Inc., 1977.

(37) C. H. Hun and Y. F. Chao. (Q. C. Xu, trans.) The Fundamentals of Acoustic Theory. Beijing, China: Defense Industrial Publishing Company, 1981.

(38) A. E. Semple and W. Thompson Jr. Improvements to the Transfer Method for Determining the Complex Dynamic Modulus of Polymer Composites. Technical Memorandum File No. TM No 85-138. Applied Research Laboratory, Pennsylvania State University Aug. 5, 1985.

(39) Akira Fukumoto, "The Application of Piezoelectric Ceramics in Diagnostic Ultrasound Transducers, " Ferroelectrics 40 pp. 167-187 (1982).

(40) Jeffrey H. Goll, "The Design of Broad-Band Fluid-Loaded Ultrasonic Transducers," IEEE Trans. Sonics Ultrason. SU-26(6) pp. 385-393 (1979).

(41) Charles S. Desilets, John D. Fraser, Gordon S. King, "The Design of Efficient Broad-Band Piezoelectric Transducers," IEEE Trans. Sonics Ultrason. SU-25(3) pp. 115-125 (1978).

(42) S. A. Farnow, B. A. Auld, "Acoustic Fresnel Zone Plate Transducers," Appl. Phys. Lett. 25(12) pp. 681-682 (1974).

(43) Virgil E. Bottom, Introduction to Quartz Crystal Unit Design New York: Van Nostrand Reinhold, 1981.

(44) H. F. Tiersten, "Thickness Vibrations of Piezoelectric Plates," J. Acoust. Soc. Am. 35(1) pp. 53-58 (1963).

(45) M. Onoe, H. F. Tiersten, and A. H. Meitzler, "Shift in the Location of Resonant Frequencies Caused by Large Electromechanical Coupling in Thickness-Mode Resonators," J. Acoust. Soc. Am. 35(1) pp. 36-42 (1963).

(46) IEEE Standards on Piezoelectricity The Institute of Electrical and Electronics Engineers 1978.

(47) D. C. Gazis and R. D. Mindlin, "Extensional Vibrations and Waves in a Circular Disk and Semi-Infinite Plate," J. Appl. Mech. pp. 541-547 (1960).

(48) Youhachi Yamashita, Katsunori Yokoyama, Hiroki Honda, and Takashi Takahashi, "$(Pb,Ca)((Co_{1/2},W_{1/2})Ti)O_3$ Piezoelectric Ceramics and Their Applications," Jpn. J. Appl. Phys.Supplement 20-4 pp. 183-187 (1981).

(49) Hiroshi Takeuchi, Shigeru Jyonura, Yasuo Ishikowa, and Etsuji Yamamoto, "A 7.5MHz Linear Array Ultrasonic Probe Using Modified $PbTiO_3$ Ceramics," preprint of paper presented at 1984 Ultrasonics Symposium.

(50) Hiroshi Takeuchi, Shigeru Jyomura, Etsuji Yamamoto, and Yukio Ito, "Electromechanical Properties of $(Pb, Ln)(Ti,Mn)O_3$ Ceramics (Ln = rare-earths)," J. Acoust. Soc. Am. 72(4) pp. 1114-1120 (1982).

(51) John D. Larson III, "An Acoustic Transducer Array for Medical Imaging -- Part I," Hewlett-Packard Journal pp. 17-26 (Oct. 1983).

(52) Hiroshi Takeuchi, Shigeru Jyomura, and Chitose Nakaya, "Highly Anisotropic Piezoelectric Ceramics and Their Application in Ultrasonic Probes," preprint of a paper presented at 1985 Ultrasonics Symposium.

(53) Wallace Arden Smith, "Composite Piezoelectric Materials for Ultrasonic Imaging Transducers -- A Review," preprint of a paper presented at 1986 IEEE International Symposium on Application of Ferroelectrics.

(54) K. A. Klicker, J. V. Biggers, and R. E. Newnham,"Composites of PZT and Epoxy for Hydrostatic Transducer Applications," J. Am. Cer. Soc. 64(1) pp. 5-9 (1981).

(55) Hiroshi Takeuchi and Chitose Nakaya, "PZT/Polymer Composites for Medical Ultrasonic Probes," Ferroelectrics 68 pp. 53-53 (1986).

(56) T. R. Gururaja et. al., "High Frequency Applications of PZT/Polymer Composite Materials," Ferroelectrics 39 pp. 1245-1248 (1981).

(57) Benson Carlin, Ulrasonics 2nd Ed. McGraw Hill Book Company, Inc., New York (1960).

(58) Tetsuro Tanaka, "Piezoelectric Devices in Japan," Ferroelectrics 40 pp. 167-187 (1982).

(59) C. L. Merkle, P. J. Morris, G. C. Lauchle, S. D. Deutsch, "Hydrodynamics Block Research Program-Proposal Submitted to Office of Naval Research. PSU-Cornell" April 11, 1986.

(60) A. P. Honess. The Nature, Origin, and Interpretation of the Etch Figures on Crystals. New York: John Wiley and Sons, Inc., 1927.

(61) S. G. Ellis, "Surface Studies on Single Crystal Germanium," J. Appl. Phys. 28 p. 1263 (1957).

(62) Michael F. Ehman. Surface Reactivity and Basic Etching Mechanism Studies in Germanium, Aluminum, and Uranium Dioxide. Ph. D. thesis, The Pennsylvania State University, Sept. 1970.

(63) P. R. Camp, "A Study of the Etching Rate of Single-Crystal Germanium," J. Electrochem. Soc. 102(10) pp. 586-593 (1955).

(64) Shigeru Jyomura, Iwao Matsuyama, and Gyozo Toda, "Effects of the Lapped Surface Layers on the Dielectric Properties of Ferroelectric Ceramics," J. Appl. Phys. 51(11) pp. 5838-5844 (1980).

(65) J. W. Faust, "Factors That Influence the Damaged Layer Caused by Abrasion of Si on Ge," Electrochem. Tech. 2 pp. 339-346 (1964).

(66) Edward K. W. Goo, Raja K. Mishra, and Gareth Thomas, "Transmission Electron Microscopy of $Pb(Zr_{0.52}Ti_{0.48})O_3$," J. Am. Ceram. Soc. 64(9) pp. 517-519 (1981).

(67) Ahmad Safari. Perforated PZT-Polymer Composites with 3-1 and 3-2 Connectivity for Hydrophone Applications. Ph. D. Thesis, The Pennsylvania State University, 1983.

(68) J. de Klerk, "The Generation of Sound," from Acoustical Holography, A. F. Metherell, H. M. A. El-Sum, and Lewis Larmore, Eds., New York: Plenum Press, 1969.

(69) Robert C. Weast, Ed. CRC Handbook of Chemistry and Physics, 64th Ed. Boca Raton, Florida: CRC Press, Inc., 1983.